# Revisiting the complexation of Cm(III) with aqueous phosphates: what can we learn from the complex structures using luminescence spectroscopy and ab initio simulations?

Huittinen, N. M.; Jessat, I.; Réal, F.; Vallet, V.; Starke, S.; Eibl, M.; Jordan, N.;

Originally published:

June 2021

**Inorganic Chemistry 60(2021), 10656-10673**

DOI: https://doi.org/10.1021/acs.inorgchem.1c01319

**Revisiting the complexation of Cm(III) with aqueous phosphates: what can we learn from the complex structures using luminescence spectroscopy and *ab initio* simulations?**

N. Huittinen[1], I. Jessat[1], F. Réal*[2], V. Vallet[2], S. Starke[3], M. Eibl[1], N. Jordan*[1]

[1]Helmholtz - Zentrum Dresden - Rossendorf, Institute of Resource Ecology, Bautzner Landstraße 400, 01328 Dresden, Germany

[2]University of Lille, CNRS, UMR 8523 - PhLAM - Physique des Lasers Atomes et Molécules, F -59000 Lille, France

[3]Helmholtz - Zentrum Dresden - Rossendorf, Computational Science Group (FWCC), Department of Information Services and Computing (FWC), Bautzner Landstraße 400, 01328 Dresden, Germany

***corresponding authors:**

*Phone: +49 351 260 2148, E-mail: n.jordan@hzdr.de*

*Phone: +33 3 2033 5929, E-mail: florent.real@univ-lille.fr*

**keywords:**

Cm(III), phosphate, complexation, luminescence, temperature, *ab initio*

**Abstract**

The coordination chemistry of Cm(III) with aqueous phosphates was investigated by means of laser–induced luminescence spectroscopy and *ab initio* simulations.

For the first time, in addition to the presence of $Cm(H_2PO_4)^{2+}$, the formation of $Cm(H_2PO_4)_2^{+}$ was unambiguously established from the luminescence spectroscopic data collected at various $H^+$ concentrations ($-\log_{10}[H^+]$ = 2.52, 3.44, and 3.65), ionic strengths (0.5 – 3.0 $mol \cdot L^{-1}$ $NaClO_4$), and temperatures (25 – 90 °C). Complexation constants for both species were derived and extrapolated to standard conditions using the specific ion interaction theory.

The molal enthalpy $\Delta_R H_m^0$ and molal entropy $\Delta_R S_m^0$ of both complexation reactions were derived using the integrated van't Hoff equation, and indicated an endothermic and entropy driven complexation. For the $Cm(H_2PO_4)_2^{+}$ complex, a more satisfactory description could be obtained when including the molal heat capacity term.

While monodentate binding of the $H_2PO_4^-$ ligand(s) to the central curium ion was found to be the most stable configuration for both complexes in our *ab initio* simulations and luminescence lifetime analyses, a different temperature–dependent coordination to hydration water molecules could be deduced from the electronic structure of the Cm(III)–phosphate complexes. More precisely, where the $Cm(H_2PO_4)^{2+}$ complex could be shown to retain an overall coordination number of 9 over the entire investigated temperature range, a coordination change from 9 to 8 was established for the $Cm(H_2PO_4)_2^{+}$ species with increasing temperature.

## 1 Introduction

Actinides are of great importance for the safety case of final waste repositories, where Am and especially Pu will dominate the long–term radiotoxicity of spent nuclear fuel (SNF). Under conditions prevailing in deep underground repositories for SNF and high–level waste (HLW) streams, these actinides are found in the trivalent and tetravalent oxidation states, of which the former one is more soluble, and therefore, potentially more mobile. The +III oxidation state is the prevailing one in the lanthanide series, members of the Rare Earth Elements (REE), playing a major role in multiple high–technology products. In addition, these REE and especially europium are very often taken as chemical analogues for the trivalent actinides.

Inorganic phosphates (mainly orthophosphates) in the environment originate from the natural decomposition or the solubilization mediated by microbial processes of phosphate–containing rocks and minerals.[1, 2] Anthropogenic sources such as fertilizer runoff and the use of phosphate–based detergents locally add to the phosphorous content in the surroundings.[3-6] In addition, phosphate–containing glasses or crystalline phosphate–based ceramics such as the monazites ($Ln$PO$_4$) may be used for the immobilization of HLW streams for safe storage in deep underground repositories in the future,[7-10] which would increase the occurrence of phosphate in the deep subsurface. In the field of REE mining, crystalline phosphate minerals such as monazites play a major role as lanthanide sources.[11, 12]

The coordination chemistry of 4f (lanthanides) and 5f (actinides) elements, particularly with a strong inorganic ligand such as phosphate, is an important factor governing their environmental behavior and subsequently their mobility in the (sub)surface.[13-15] Thus, in order to predict the mobility of f–elements in natural aquatic systems in the presence of phosphate, reliable thermodynamic data such as complexation constants, solubility products, as well as enthalpies and entropies of reaction are required. Depending on the f–element in question, soluble complexes may form in solution, which do not adhere on solid phases due to *e.g.*, charge constraints, consequently increasing the mobility of the metal ion in the surrounding. Alternatively, the solubility of an f–element–bearing phosphate solid phase can be exceeded, leading to precipitation and, potentially, to the immobilization of the lanthanide or actinide. This consequently renders any experimental determination of the aqueous speciation of f–elements in the presence of orthophosphates extremely difficult. However, the actinide curium(III) which exhibits remarkable luminescence properties, allows overcoming this issue using sub micro–molar concentrations for speciation and structural studies by applying

luminescence spectroscopy. Thus, the following discussion will focus on the actinide–phosphate coordination chemistry.

As already recognized in our previous investigation dealing with the complexation of Eu(III) and Cm(III) with aqueous phosphates at elevated temperatures,[16] studies concerning the complexation reactions of trivalent actinides with various phosphate ligands, *i.e.*, $H_2PO_4^-$, $HPO_4^{2-}$, or $PO_4^{3-}$, are rather scarce. Most of the available data exists for the $AnH_2PO_4^{2+}$ complex with some literature found for $AnHPO_4^+$ (Table 1).

Table 1: Published complexation constants at infinite dilution ($\log_{10}$ β°) for Cm(III)– and Am(III)–phosphate complexes.

| Literature | Method | Complex | $\log_{10}\beta^0$ | T [°C] | Complex formation reaction |
|---|---|---|---|---|---|
| Curium | | | | | |
| Jordan et al. (2018)[16] | [a]TRLFS ($\lambda_{exc} = 396.6$ nm) | $Cm(H_2PO_4)^{2+}$ | [b]2.59 ± 0.19<br>[b]2.73 ± 0.16<br>[b]2.83 ± 0.24<br>[b]2.96 ± 0.16<br>[b]3.11 ± 0.16 | 25<br>40<br>50<br>60<br>80 | $Cm^{3+} + H_2PO_4^- \rightleftharpoons Cm(H_2PO_4)^{2+}$ |
| Moll et al. (2011)[17] | [a]TRLFS ($\lambda_{exc} = 396$ nm) | $Cm(H_2PO_4)^{2+}$<br>$Cm(HPO_4)^+$ | 2.46 ± 0.13<br>6.21 ± 0.80 | [c]R.T. | $Cm^{3+} + H_2PO_4^- \rightleftharpoons Cm(H_2PO_4)^{2+}$<br>$Cm^{3+} + HPO_4^{2-} \rightleftharpoons Cm(HPO_4)^+$ |
| Morgenstern (1997)[18] | [a]TRLFS | $Cm(H_2PO_4)^{2+}$ | [d]2.71 ± 0.04 | [c]R.T. | $Cm^{3+} + H_2PO_4^- \rightleftharpoons Cm(H_2PO_4)^{2+}$ |
| Moskvin (1969)[19] | [e]N.A. | $Cm(H_2PO_4)^{2+}$<br>$Cm(H_2PO_4)_2^+$<br>$Cm(H_2PO_4)_3^0$<br>$Cm(H_2PO_4)_4^-$ | 2.40<br>3.60<br>5.61<br>6.20 | [e]N.A. | $Cm^{3+} + H_2PO_4^- \rightleftharpoons Cm(H_2PO_4)^{2+}$<br>$Cm^{3+} + 2\ H_2PO_4^- \rightleftharpoons Cm(H_2PO_4)_2^+$<br>$Cm^{3+} + 3\ H_2PO_4^- \rightleftharpoons Cm(H_2PO_4)_3^0$<br>$Cm^{3+} + 4\ H_2PO_4^- \rightleftharpoons Cm(H_2PO_4)_4^-$ |
| Americium | | | | | |
| Rao et al. (1986)[20] | Solvent extraction | $Am(H_2PO_4)^{2+}$<br>$Am(HPO_4)^+$ | 2.13 ± 0.08<br>4.14 ± 0.08 | 30 | $Am^{3+} + H_2PO_4^- \rightleftharpoons Am(H_2PO_4)^{2+}$<br>$Am^{3+} + HPO_4^{2-} \rightleftharpoons Am(HPO_4)^+$ |
| Borisov et al. (1966)[21] | Cation exchange | $Am(H_2PO_4)^{2+}$ | 2.51 | 20 ± 2 | $Am^{3+} + H_2PO_4^- \rightleftharpoons Am(H_2PO_4)^{2+}$ |
| Moskvin (1969)[19] | [e]N.A. | $Am(H_2PO_4)^{2+}$<br>$Am(H_2PO_4)_2^+$<br>$Am(H_2PO_4)_3^0$<br>$Am(H_2PO_4)_4^-$ | 2.39<br>3.63<br>5.62<br>6.30 | [e]N.A. | $Am^{3+} + H_2PO_4^- \rightleftharpoons Am(H_2PO_4)^{2+}$<br>$Am^{3+} + 2\ H_2PO_4^- \rightleftharpoons Am(H_2PO_4)_2^+$<br>$Am^{3+} + 3\ H_2PO_4^- \rightleftharpoons Am(H_2PO_4)_3^0$<br>$Am^{3+} + 4\ H_2PO_4^- \rightleftharpoons Am(H_2PO_4)_4^-$ |

| | | | | | |
|---|---|---|---|---|---|
| Lebedev et al. (1979)[22] | Spectrophotometry | $Am(H_2PO_4)^{2+}$ | [f]2.73 ± 0.06 | 23 ± 2 | $Am^{3+} + H_2PO_4^- \rightleftharpoons Am(H_2PO_4)^{2+}$ |
| | | $Am(H_2PO_4)_2^+$ | [f]3.72 ± 0.02 | | $Am^{3+} + 2\ H_2PO_4^- \rightleftharpoons Am(H_2PO_4)_2^+$ |

[a]TRLFS: time resolved laser induced fluorescence spectroscopy
[b]recalculated using the values published by Jordan et al. (2018)[16] and the $\log_{10}\ \beta^0$ and $\Delta_R H_m^0$ values for the reaction $H^+ + H_2PO_4^- \rightleftharpoons H_3PO_4$ at each temperature from Lemire et al. (2020)[23]
[c]R.T.: room temperature
[d]from the value recalculated by Moll et al. (2011)[17] for the equilibrium $Cm^{3+} + 2H^+ + PO_4^{3-} \rightleftharpoons Cm(H_2PO_4)^{2+}$
[e]N.A.: not available
[f]: As mentioned by Silva et al. (1995)[24], the reaction involves exchange between ligands and solvation water molecules and the equilibrium constant was corrected for changes in water activity

Note that the values of Moskvin (1971)[25] determined by ion exchange are not indicated in Table 1 since only conditional constants at I = 1.0 mol·L$^{-1}$ $NH_4Cl$ were reported and not all the required ion interaction coefficients are available for the extrapolation to infinite dilution (Lemire et al. (2020)).[23] Note also that the values of the stepwise conditional complexation constants reported by Moskvin (1969)[19] for Am(III) and Cm(III) do not show the expected decrease with the increase of $H_2PO_4^-$ ligands. For the $Am(H_2PO_4)^{2+}$ complex, Silva et al. (1995)[24] (Nuclear Energy Agency (NEA) Thermochemical Database (TDB) Project, vol. 2) recommended a $\log_{10}\ \beta°$ value at 25 °C, based on the solvent extraction study of Rao et al. (1986).[20] Later Morgenstern (1997)[18] and Moll et al. (2011)[17] reported a $\log_{10}\ \beta°$ value of very similar magnitude for $Cm(H_2PO_4)^{2+}$, derived from luminescence spectroscopic investigations, which was recently confirmed.[16]

For *An*$HPO_4^+$ published literature values for the complexation constant deviate by more than two orders of magnitude. Furthermore, no recommended value from the NEA–TDB for the complexation constant of this *An*–phosphate complex exists, as the stoichiometry of the complex has not been unambiguously proven in the existing literature. Further complexes such as *An*$(H_2PO_4)_3^0$ and *An*$(H_2PO_4)_4^-$ were also reported, but a spectroscopic verification and confirmation of the stoichiometry of the proposed complexes is still missing. In addition, structural data in terms of denticity, bond lengths and their character, together with the coordination number of the central ion (f–element) of the accepted actinide phosphate complexes does, to the best of our knowledge, not exist. Despite that spectroscopic tools have been used for the derivation of thermodynamic data, the changes occurring in the electronic structure of the actinide–complexes under different chemical conditions have not been used to derive such structural data.

As briefly mentioned, our previous study investigated the complexation of Cm(III) with aqueous phosphates at acidic pH ($-\log[H^+] = 1.00$) using luminescence spectroscopy. At this very acidic pH, only the $H_2PO_4^-$ ligand is present in solution in addition to non–dissociated

phosphoric acid ($H_3PO_4$), which facilitated the interpretation of collected spectroscopic data. By conducting the experiments at several ionic strengths (I = 0.6–3.1 mol·$L^{-1}$) the specific ion interaction theory (SIT) could be used for the extrapolation of the obtained complexation constants to infinite dilution and to extract the first experimentally determined ion interaction coefficient $\varepsilon(Cm(H_2PO_4)^{2+}; ClO_4^-)$. Temperature–dependent investigations in the range 25 °C– 80 °C enabled the extraction of first thermodynamic data for the $Cm(H_2PO_4)^{2+}$ complex. The results showed an increase of complexation with increasing temperature resulting in both a positive molal enthalpy ($\Delta_R H°_m$) and entropy ($\Delta_R S°_m$) of reaction.

In the present study we have extended the range of $-\log_{10}[H^+]$ from 2.52 up to 3.65. This increases the amount of $HPO_4^{2-}$ in solution and subsequently the possibility for $Cm(HPO_4)^+$ complex formation. Namely, one can gain an insight into the Cm(III)–phosphate speciation as a function of pH and total phosphate concentration, under conditions where solid Cm(III)–phosphate precipitation can be avoided. The complexation studies were conducted at several ionic strengths (I = 0.5–3.0 mol·$L^{-1}$ $NaClO_4$) to allow for the use of the SIT approach for the extrapolation of the conditional $\log_{10} \beta$ to infinite dilution and to extract ion interaction parameters ($\varepsilon$) for the found species. In addition, temperature–dependent studies were conducted at $-\log_{10}[H^+] = 2.52$ from 25 °C up to 90 °C at I = 1.0 mol·$L^{-1}$ to extract molal enthalpy and entropy of reaction for the Cm(III)–phosphate species present in solution using the integrated van't Hoff equation.

To understand the underlying reasons for the increased stability of the Cm–phosphate complexes at elevated temperature, such as changes in the first–shell coordination, spectroscopic data has been evaluated and compared to *ab initio* simulations of the electronic states of these solution species in 9–fold and 8–fold coordination. Electronic ground–state calculations were used for a qualitative description of the energetic stabilities of the various solution species at different temperatures, while the computations of electronic excited states have been used to link the observed luminescence features with the stoichiometry of the complexes and the first–shell coordination around the $Cm^{3+}$ cation.

# 2 Results

## 2.1 Influence of pH and ionic strength on Cm(III) complexation with phosphate at 25 °C

### *2.1.1 Luminescence spectroscopy*

Cm(III) ($1.15\times10^{-7}$ mol·L$^{-1}$) luminescence emission spectra collected from phosphate containing solutions with [$\Sigma(PO_4)$] ranging from zero to 0.055 mol·L$^{-1}$ at 25°C, $-\log_{10}[H^+] = 2.52$ and I = 1.0 mol·L$^{-1}$ are presented in Figure 1, top, left. The data corresponding to [Cm(III)] = $1.15\times10^{-8}$ mol·L$^{-1}$, $[\Sigma(PO_4)]_{max}$ = 0.07 mol·L$^{-1}$ and I = 1.0 mol·L$^{-1}$ at the higher proton concentration of $-\log_{10}[H^+] = 3.44$ is presented in Figure 1 top, right.

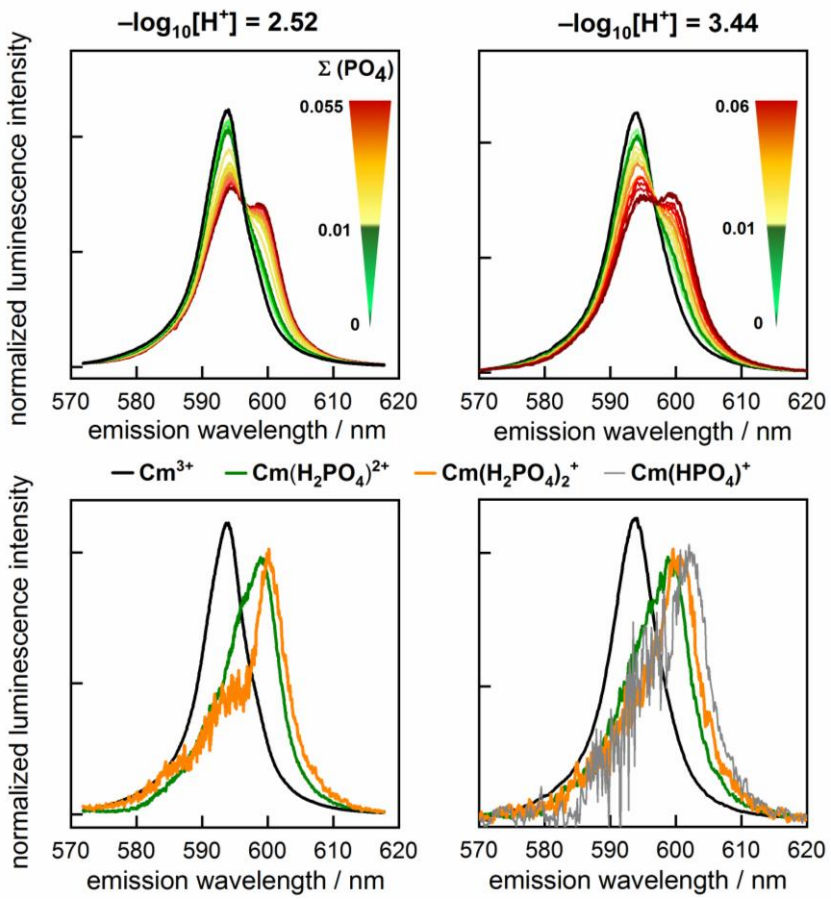


Figure 1: Top: Cm(III) luminescence emission spectra at 25 °C, I = 1.0 mol·L$^{-1}$ in the presence of $\Sigma(PO_4)$ = 0–0.055 mol·L$^{-1}$ at $-\log_{10}[H^+]$ = 2.52 (left) and [$\Sigma(PO_4)$] = 0–0.07 mol·L$^{-1}$ at $-\log_{10}[H^+]$ = 3.44 (right). Bottom: Pure component spectra for the Cm(III) aquo ion and various Cm(III)–phosphate complexes.

Both sets of recorded luminescence spectra show a clear shift toward longer wavelengths with increasing phosphate concentration, pointing toward a progressing complexation reaction in solution between Cm(III) and the phosphate ligands. To obtain pure component spectra of the individual species as well as their relative distributions and luminescence intensity factors, the

measured multicomponent spectra were deconvoluted as explained in section 5.3. At the higher proton concentration of $-\log_{10}[H^+] = 2.52$, two components in addition to the non–complexed Cm(III) aquo ion could be obtained (Figure 1, bottom, left). The peak positions of the two Cm(III)–phosphate complexes are found at 599.2 nm and 600.4 nm. The former spectrum is identical, both in terms of the peak position and the overall peak shape, to the one obtained in our previous study for the $Cm(H_2PO_4)^{2+}$ complex [16]. Thus, the first Cm–phosphate species obtained in the present study can be assigned to the 1:1 ($Cm^{3+}$:$H_2PO_4^-$) $Cm(H_2PO_4)^{2+}$ species. The second species, however, may arise either from additional complexation of Cm with the $H_2PO_4^-$ ligand resulting in *e.g.*, a 1:2 complex ($Cm(H_2PO_4)_2^+$) or from complexation with $HPO_4^{2-}$, resulting in $Cm(HPO_4)^+$. By increasing the solution pH, an additional Cm(III)–phosphate complex can be identified from the deconvoluted luminescence spectra with a peak maximum at 601.9 nm (Figure 1, bottom, right). The signal–to–noise ratio of the obtained spectrum is very low, owing to the very low amount of this species in solution. As this third species is not present in the lower pH–regime for comparable phosphate concentrations, we tentatively assign the species to the $Cm(HPO_4)^+$ complex. Subsequently, the aforementioned Cm(III)–phosphate species, present also at lower pH, is likely to be the $Cm(H_2PO_4)_2^+$ complex. A detailed discussion of the phosphate speciation and the stoichiometries of the derived complexes will be given in section 2.1.2.

From the obtained pure component spectra, the relative distributions of the individual species were calculated, taking into account the different luminescence quantum yields of the species relative to the aquo ion (LI factors). The corrected species distributions using LI factors of 1.00 for the aquo ion and 0.89 ± 0.14, 0.97 ± 0.22, and 1.15 ± 0.62 for the phosphate complexes 1 ($Cm(H_2PO_4)^{2+}$), 2 ($Cm(H_2PO_4)_2^+$), and 3 ($Cm(HPO_4)^+$), respectively, are presented in Figure 2 for $-\log_{10}[H^+] = 2.52$ (top, left) and $-\log_{10}[H^+] = 3.44$ (bottom, left). Species distributions for other ionic strengths at the two investigated pH–values are available in the Figure S1 in the supporting information (SI).

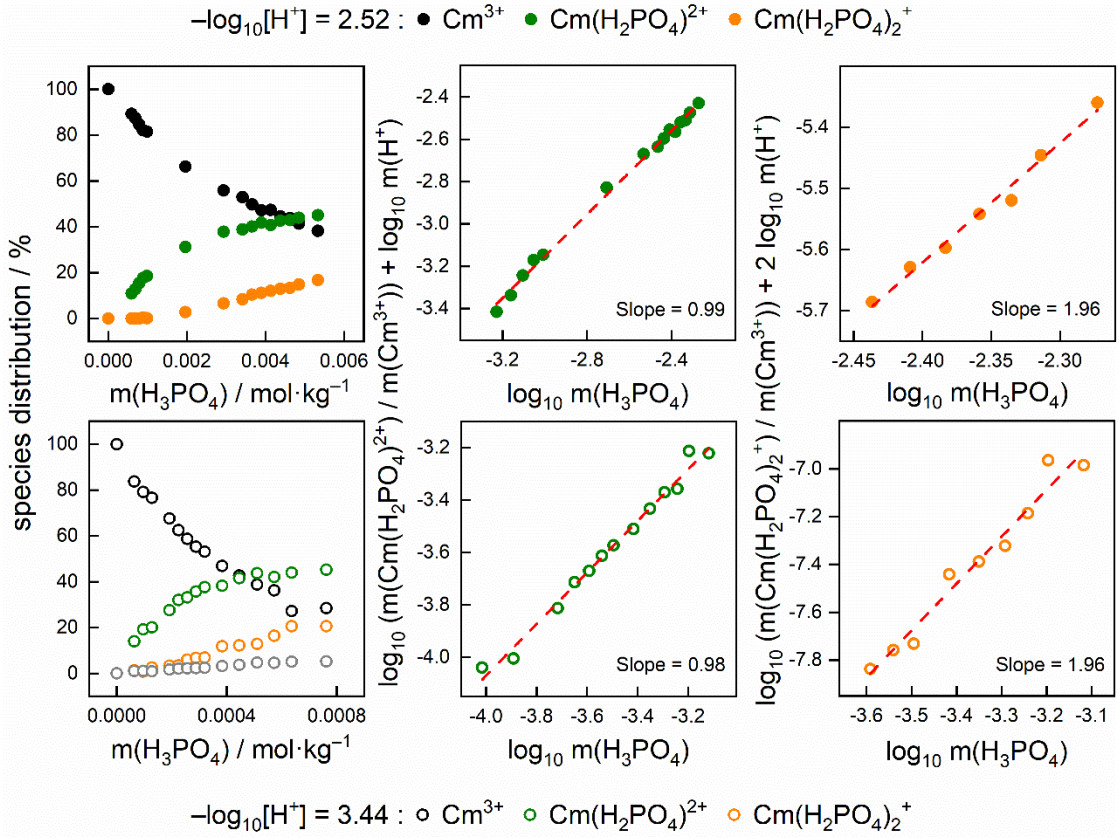


Figure 2: Cm(III) species distribution at 25 °C, I = 1.0 mol·L$^{-1}$ in the presence of [Σ($PO_4$)] = 0–0.055 mol·L$^{-1}$ at –log$_{10}$[$H^+$] = 2.52 (top, left) and [Σ($PO_4$)] = 0–0.07 mol·L$^{-1}$ at –log$_{10}$[$H^+$] = 3.44 (bottom, left). The corresponding slope analyses obtained from the species distributions are shown for species 1 ($Cm(H_2PO_4)^{2+}$), middle, and species 2 ($Cm(H_2PO_4)_2^+$), right.

As expected, the amount of Cm(III)–phosphate complexes is slightly higher at –log$_{10}$[$H^+$] = 3.44 than at –log$_{10}$[$H^+$] = 2.52. In addition, the third Cm(III)–phosphate complex ($Cm(HPO_4)^+$) is only present at the higher pH–value in the investigated phosphate–concentration range. The reason for the enhanced phosphate–complex formation with increasing pH can be attributed to the increasing amount of $H_2PO_4^-$ and $HPO_4^{2-}$ ligands in solution as the phosphoric acid ($H_3PO_4$) dissociates. In agreement with our previous study, an increase of the ionic strength leads to a slight increase of the amount of Cm(III)–phosphate complexes in solution (see SI, Figure S1). The derivation and the magnitude of the Cm(III)–phosphate complexation constants will be discussed below in section 2.1.2.

Luminescence lifetimes (τ), which can provide information on the number of coordinating water molecules around the Cm(III) cation using Eq. 1 proposed by Kimura and Choppin,[26] were collected for selected samples at both investigated pH–values.

$$n(H_2O) = \frac{0.65}{\tau(ms)} - 0.88 \qquad \text{(Eq. 1)}$$

The obtained lifetime curves (natural logarithm of the integrated luminescence intensity vs. delay time between the laser pulse and camera gating) all decay mono–exponentially despite

the presence of at least two components in all measured samples (see SI, Figure S2). This implies that the dynamic exchange reactions in the Cm(III) hydration sphere between coordinated water and phosphate ligands occur faster than the luminescence decay of the individual species. In order to draw conclusion on the coordination of the phosphate ligands via the amount of coordinating water around the Cm(III) ion in solution, theoretical lifetimes were calculated according to Eq. 2, assuming a lifetime of 68 µs for the Cm(III) aquo ion (9 $H_2O$), 73 µs for $Cm(H_2PO_4)^{2+}$ (8 $H_2O$) and 83 µs for $Cm(H_2PO_4)_2^{+}$ and $Cm(HPO_4)^{+}$ (7 $H_2O$).

$$\tau(\text{calc.}) = a \cdot 68\ \mu s + b \cdot 73\ \mu s + (c + d) \cdot 83\ \mu s \qquad \text{(Eq. 2)}$$

The factors a–d are the fractions of the individual species determined from the experimentally derived species distributions (non–corrected for relative differences in the luminescence quantum yield). These assumed lifetimes imply monodentate coordination of the $H_2PO_4^-$ ligand, where each coordinated ligand replaces one $H_2O$ in the first hydration sphere and bidentate coordination of $HPO_4^{2-}$ resulting in the replacement of two $H_2O$ around the Cm(III) cation. The results of the experimental fits and the calculated lifetimes are summarized in Table 2.

Table 2: Experimentally determined and calculated luminescence lifetimes of Cm(III)–phosphate solutions at 25 °C.

| $-\log_{10}[H^+]$ | $[\Sigma(PO_4)]$ mol·L$^{-1}$ | Derived fractions (a–d) of Cm(III) species* | τ(exp.) µs | τ(calc.) µs |
|---|---|---|---|---|
| 2.52 | 0.009 | a = 0.83, b = 0.17 | 68 ± 2 | 69 |
| 2.52 | 0.02 | a = 0.66, b = 0.29, c = 0.05 | 70 ± 2 | 70 |
| 2.52 | 0.045 | a = 0.43, b = 0.41, c = 0.16 | 71 ± 2 | 72 |
| 3.44 | 0.02 | a = 0.57, b = 0.33, c = 0.07, d = 0.03 | 71 ± 3 | 71 |
| 3.44 | 0.04 | a = 0.38, b = 0.42, c = 0.13, d = 0.07 | 73 ± 2 | 73 |
| 3.44 | 0.06 | a = 0.27, b = 0.43, c = 0.22, d = 0.08 | 76 ± 3 | 75 |

* a($Cm^{3+}$), b($Cm(H_2PO_4)^{2+}$), c($Cm(H_2PO_4)_2^{+}$), d($Cm(HPO_4)^{+}$), a+b+c+d = 1

At a first glance, the experimental and theoretical values are in very good agreement with one another. This would imply that the assumed coordination of the phosphate ligands to the Cm(III) cation follows the denticity proposed above, i.e., monodentate to the $H_2PO_4^-$ ligand and bidentate to $HPO_4^{2-}$. Due to the uncertainties of the experimentally determined lifetimes

in combination with the very moderate changes of the lifetimes as a result of phosphate complexation where only one or two water molecules are removed from the Cm(III) hydration sphere, computational studies were performed to support these conclusions (see section 2.3).

### *2.1.2 Determination of the conditional $log_{10}$ *$\beta$ and $log_{10}$ *$\beta^0$ at 25 °C*

Determination of the conditional complexation constants at 25 °C

From the deconvolution of the luminescence spectra at the different $-\log_{10}[H^+]$ and ionic strengths investigated at 25 °C the molar concentrations of the $Cm^{3+}$ aquo ion and the $Cm(H_2PO_4)^{2+}$ and $Cm(H_2PO_4)_2^+$ complexes could be obtained. These concentrations were at first converted to the molal scale using the density of $NaClO_4$, the background electrolyte, reported by Söhnel and Novotný.[27] These molalities were used to calculate the conditional complexation constants $\log_{10}$ *$\beta$ assuming the two following equilibria:

$Cm^{3+} + H_3PO_4 \rightleftharpoons Cm(H_2PO_4)^{2+} + H^+$ (R–1), $\log_{10}{}^*\beta_1$

$Cm^{3+} + 2\ H_3PO_4 \rightleftharpoons Cm(H_2PO_4)_2^+ + 2\ H^+$ (R–2), $\log_{10}{}^*\beta_2$

The asterisk is used here to represent a complexation reaction involving the deprotonation of the $H_3PO_4$ ligand.[23]

In all experiments, the molality of Cm(III) was orders of magnitude lower than the one of phosphoric acid. Thus, one can assume that the speciation of the different phosphate ligands was not significantly impacted by the complexation with Cm(III). By applying the law of mass action, the following expressions of the conditional complexation constant were obtained:

$$\log_{10}{}^*\beta_1 = \log_{10}\left(\frac{m_{Cm(H_2PO_4)^{2+}} \cdot m_{H^+}}{m_{Cm^{3+}} \cdot m_{H_3PO_4}}\right) \qquad \text{(Eq. 3)}$$

$$\log_{10}{}^*\beta_2 = \log_{10}\left(\frac{m_{Cm(H_2PO_4)_2^+} \cdot (m_{H^+})^2}{m_{Cm^{3+}} \cdot (m_{H_3PO_4})^2}\right) \qquad \text{(Eq. 4)}$$

Based on Eq. 3 and Eq. 4, the terms $\log_{10}\frac{m_{Cm(H_2PO_4)^{2+}}}{m_{Cm^{3+}}} + \log_{10} m_{H^+}$ and $\log_{10}\frac{m_{Cm(H_2PO_4)_2^+}}{m_{Cm^{3+}}} + 2\ \log_{10} m_{H^+}$ were exemplarily plotted as a function of $\log_{10} m_{H_3PO_4}$ at an ionic strength of 1 mol·$L^{-1}$ (Figure 2, middle and right). The results of the slope analysis for all other conditions are given in the SI (Figure S3 for $Cm(H_2PO_4)^{2+}$ and Figure S4 for $Cm(H_2PO_4)_2^+$). The slopes were systematically close to one and two, respectively, confirming the postulated formation of the $Cm(H_2PO_4)^{2+}$ and $Cm(H_2PO_4)_2^+$ complexes. Note that the individual slopes were just aiming at verifying the stoichiometry of the proposed complexes and were not used

for the derivation of the conditional complexation constants. For the second Cm–phosphate species, the formation of $Cm(HPO_4)^+$ based on the following equilibrium:

$$Cm^{3+} + H_3PO_4 \rightleftharpoons Cm(HPO_4)^+ + 2H^+$$

was also considered but eventually not retained. Indeed, the slope analysis led to a slope of 2 (Figure 2, right) and not one.

At constant $m_{H^+}$ and ionic strength, a conditional complexation constant was calculated at each phosphate concentration using the law of mass action. These values were averaged and correspond to the conditional $\log_{10}$ *β summarized in Table 3.

Table 3. Thermodynamic conditional complexation constants for the formation of $Cm(H_2PO_4)^{2+}$ and $Cm(H_2PO_4)_2^+$ at 25 °C at varying ionic strengths ($\log_{10}$ *β in the molal scale).

| Ionic strength (mol·L$^{-1}$) | Ionic strength (mol·kg$^{-1}$) | –log[H$^+$] | $\log_{10}{}^*\beta_1$ | $\log_{10}{}^*\beta_2$ |
|---|---|---|---|---|
| 0.5 | 0.51 | 2.52 | −0.20 ± 0.10 | −0.87 ± 0.15 |
| 0.6 | 0.62 | 1.00 | −0.25 ± 0.22[a] | |
| 1.0 | 1.05 | 2.52 | −0.16 ± 0.15 | −0.82 ± 0.25 |
| 1.0 | 1.05 | 3.44 | −0.08 ± 0.15 | −0.68 ± 0.25 |
| 1.1 | 1.16 | 1.00 | −0.14 ± 0.10[a] | |
| 2.0 | 2.21 | 2.52 | −0.13 ± 0.15 | −0.57 ± 0.30 |
| 2.1 | 2.33 | 1.00 | −0.06 ± 0.11[a] | |
| 2.4 | 2.71 | 3.44 | 0.02 ± 0.20 | −0.57 ± 0.35 |
| 3.0 | 3.50 | 3.65 | 0.05 ± 0.20 | −0.43 ± 0.40 |

[a] Values were taken from Jordan et al. (2018)[16]

The highest standard deviation for the $\log_{10}$ *β obtained within all experiments in this study was 0.07. However, one can see that the uncertainties in Table 3 are higher, and the underlying reason will be explained. As already mentioned in Jordan et al. (2018),[16] the SIT database from ThermoChimie suffers from a conflict between the ion interaction model and the ion association model. Indeed, the ThermoChimie database contains both complexation constants for the formation of several ion pairs between $Na^+$ and the phosphate ligands, i.e.

$NaH_2PO_4^0$, $Na(HPO_4)^-$ and $NaPO_4^{2-}$ as well as the $\varepsilon(Na^+;H_2PO_4^-)$, $\varepsilon(Na^+;HPO_4^{2-})$, and $\varepsilon(Na^+;PO_4^{3-})$ ion interaction coefficients. Resolving this contradiction needs efforts which would exceed the scope of this work. Consequently, all molalities of the free $H_3PO_4$ were calculated again by removing the formation constants of these three ion pairs from the ThermoChimie database and the respective conditional complexation constants $\log_{10}$ *β were derived. Eventually, a pragmatic approach was used, i.e. the uncertainty of the conditional complexation constants summarized in Table 3 were increased to allow overlap with the complexation constants obtained without considering the formation of the $NaH_2PO_4^0$, $Na(HPO_4)^-$ and $NaPO_4^{2-}$ ion pairs.

According to Table 3, increasing the ionic strength at constant $[H^+]$ or decreasing the $[H^+]$ at constant ionic strength leads to an increase of the conditional complexation constants derived at 25 °C for both $Cm(H_2PO_4)^{2+}$ and $Cm(H_2PO_4)_2^+$ complexes, in agreement with the luminescence data.

Extrapolation to infinite dilution at 25 °C

The conditional complexation constants were extrapolated to the infinite dilution state applying the SIT equation, which basic assumption is that the reactants and products of the reaction only interact with the ions of the background electrolyte. No interaction between species bearing the same charge sign is considered, whereas neutral species are also assumed to not interact with other ions. The activity coefficient of a species j (reactant or product) interacting with species k is expressed as follows:

$$\log_{10}\gamma_j = -z_j^2 D + \sum_k \varepsilon(j;k) \cdot m_k \qquad \text{(Eq. 5)}$$

where $z_j$ stands for the charge of species j, ε(j;k) represents the ion interaction coefficient between species j and species k, $m_k$ the molality of species k, and D the Debye–Hückel term:

$$D = \frac{A \cdot \sqrt{I_m}}{1 + Ba_i \cdot \sqrt{I_m}} \qquad \text{(Eq. 6)}$$

The term A is the Debye–Hückel constant. According to Lemire et al. (2020),[23] A = 0.509 $kg^{1/2} \cdot mol^{-1/2}$ at 25 °C, whereas the empirical parameter $Ba_i$ is taken as 1.5 $kg^{1/2} \cdot mol^{-1/2}$ for all temperatures up to 90 °C.[23]

The relation between the conditional complexation constant and the equilibrium complexation constant at infinite dilution is given by the following equation:

$$\log_{10} *\beta - \Delta z^2 D = \log_{10} *\beta^\circ - \Delta\varepsilon I_m \qquad \text{(Eq. 7)}$$

For the two equilibria (R–1) and (R–2) under consideration, the following expressions for Δε are obtained:

$$\Delta\varepsilon = \varepsilon(Cm(H_2PO_4)^{2+};ClO_4^-) + \varepsilon(H^+;ClO_4^-) - \varepsilon(Cm^{3+};ClO_4^-) \quad \text{(Eq. 8)}$$

$$\Delta\varepsilon = \varepsilon(Cm(H_2PO_4)_2^+;ClO_4^-) + 2\times\varepsilon(H^+;ClO_4^-) - \varepsilon(Cm^{3+};ClO_4^-) \quad \text{(Eq. 9)}$$

The interaction coefficient $\varepsilon(H^+;ClO_4^-)$ was taken from Lemire et al. (2020)[23] while $\varepsilon(Cm^{3+};ClO_4^-)$ was postulated to be equal to $\varepsilon(Am^{3+};ClO_4^-) = 0.49 \pm 0.03$ kg·mol$^{-1}$. Following the SIT formalism, all ion interaction coefficients of the uncharged species $H_3PO_4$ were set to zero [23]. $\Delta z^2 = \Sigma z^2$ (products) $- \Sigma z^2$ (reactants) was equal to −4 and −6 for reactions (R–1) and (R–2), respectively.

By plotting $\log_{10} {}^*\beta - \Delta z^2 D$ as a function of the ionic strength, a weighted linear regression provided $\log_{10} {}^*\beta^\circ$ (intercept with the y–axis) and $-\Delta\varepsilon$ (slope) (Figure 3). Detailed explanations on the performance of the weighted linear regression and the derivation of the uncertainties of the slope and intercept are available elsewhere.[16] However, in the present study, we assumed the individual error variance to be known up to a constant of proportionality k[28] and use the quantiles of the student t–distribution with n−2 degrees of freedom to compute intervals of confidence.

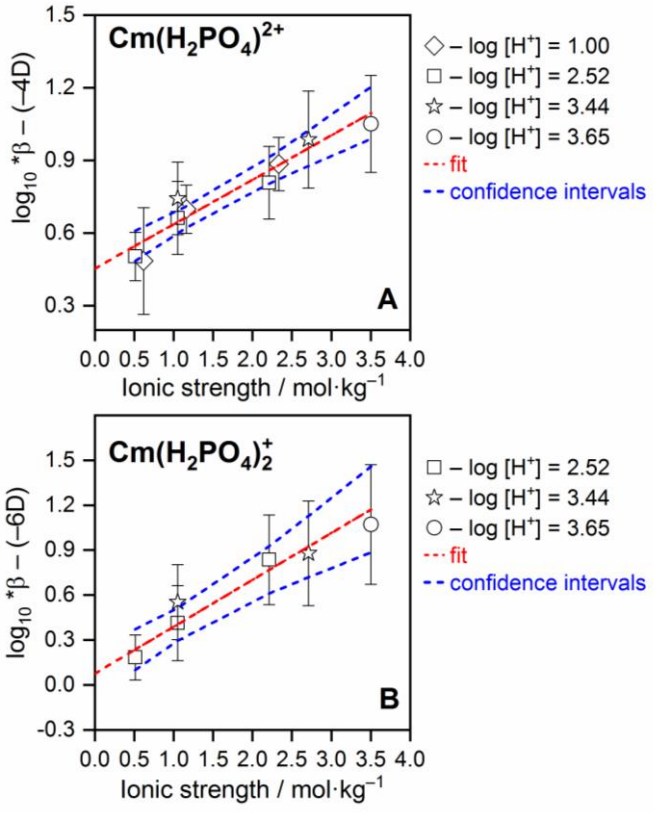

Figure 3: Linear SIT regression plot for the $Cm(H_2PO_4)^{2+}$ (A) and $Cm(H_2PO_4)_2^{+}$ (B) complexes at 25 °C.

The slopes of the SIT regression for the $Cm(H_2PO_4)^{2+}$ and $Cm(H_2PO_4)_2^{+}$ complexes were found to be 0.18 ± 0.02 and 0.31 ± 0.04, respectively. The obtained $\log_{10}$ *β° and $\varepsilon(Cm(H_2PO_4)^{2+};ClO_4^-)$ and $\varepsilon(Cm(H_2PO_4)_2^{+};ClO_4^-)$ ion interaction coefficients are summarized in Table 4.

Table 4: Complexation constants at infinite dilution ($\log_{10}$ *β°) for the $Cm(H_2PO_4)^{2+}$ and $Cm(H_2PO_4)_2^{+}$ complexes and ion interaction coefficients $\varepsilon(Cm(H_2PO_4)^{2+};ClO_4^-)$ and $\varepsilon(Cm(H_2PO_4)_2^{+};ClO_4^-)$ at 25 °C.

| Reaction | $\log_{10}$ *β° | $\varepsilon(Cm(H_2PO_4)_n^{(3-n)+};ClO_4^-)$ (kg·mol$^{-1}$) |
|---|---|---|
| $Cm^{3+} + H_3PO_4 \rightleftharpoons Cm(H_2PO_4)^{2+} + H^+$ | 0.45 ± 0.04 | 0.17 ± 0.04 (n = 1) |
| $Cm^{3+} + 2\ H_3PO_4 \rightleftharpoons Cm(H_2PO_4)_2^{+} + 2\ H^+$ | 0.08 ± 0.07 | −0.10 ± 0.06 (n = 2) |

The uncertainties on the ion interaction coefficients ε were calculated based on the recommendations in Appendix C in the most recent NEA volume.[23]

$$\sigma_{\varepsilon(Cm(H_2PO_4)^{2+};ClO_4^-)} = \sqrt{(\sigma_{\Delta\varepsilon})^2 + \sigma(\varepsilon(H^+;ClO_4^-))^2 + \sigma(\varepsilon(Cm^{3+};ClO_4^-))^2} \quad \text{(Eq. 10)}$$

$$\sigma_{\varepsilon(Cm(H_2PO_4)_2^{+};ClO_4^-)} = \sqrt{(\sigma_{\Delta\varepsilon})^2 + (2 \cdot \sigma(\varepsilon(H^+;ClO_4^-)))^2 + \sigma(\varepsilon(Cm^{3+};ClO_4^-))^2} \quad \text{(Eq. 11)}$$

## 2.2 Influence of temperature on the complexation of Cm(III) by phosphate

### *2.2.1 Luminescence spectroscopy*

For the extraction of thermodynamic data for the two identified complexes, $Cm(H_2PO_4)^{2+}$ and $Cm(H_2PO_4)_2^{+}$, temperature–dependent luminescence spectroscopic measurements were conducted for the sample row prepared at $-\log_{10}[H^+]$ = 2.52 and I = 1.0 mol·L$^{-1}$ in the temperature–range between 25 °C and 90 °C as explained in section 5.1.2. Cm(III) emission spectra recorded at two different phosphate concentrations as a function of temperature are presented in Figure S5. Similarly to the data collected at 25 °C, a spectral deconvolution of the measured emission spectra was carried out for each temperature, yielding pure component spectra as well as FI–corrected species distributions. The species distribution at 90 °C is presented in Figure 4 (closed symbols), together with the 25 °C data (open symbols).

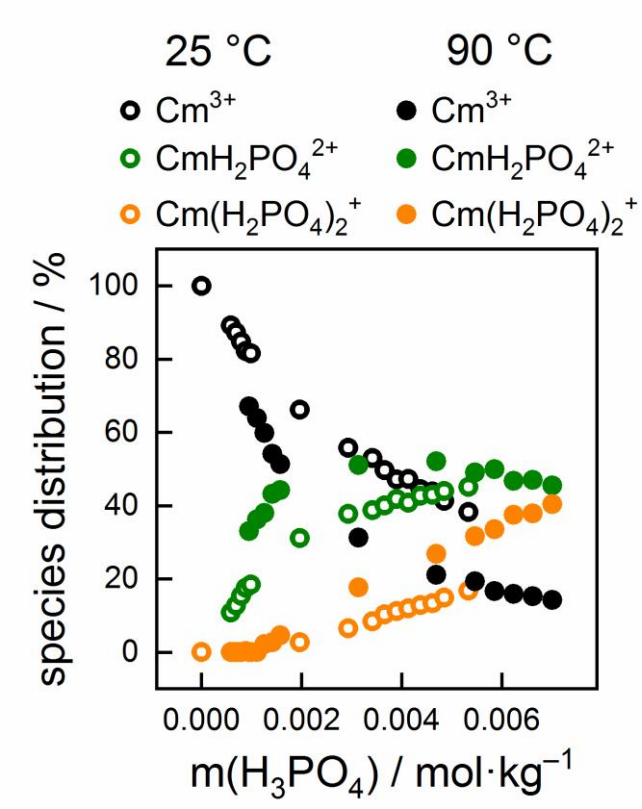


Figure 4: Comparison of the Cm(III) species distribution at 25 °C and 90 °C in solutions containing 0–0.055 mol·L$^{-1}$ [Σ($PO_4$)] at –log$_{10}$[$H^+$] = 2.52 and I = 1.0 mol·L$^{-1}$.

As evident from both the temperature–dependent Cm(III) emission spectra at constant phosphate concentration (Figure S5 in SI) and the obtained species distribution at 90 °C (Figure 4), the complexation reaction between Cm(III) and $H_2PO_4^-$ is promoted with increasing temperature. Only two phosphate complexes, described by similar pure component emission spectra as those obtained at 25 °C, were found over the entire investigated temperature range, speaking for an unchanged Cm(III)–phosphate species present in solution also at elevated temperatures.

### *2.2.2 Determination of conditional complexation constants log$_{10}$ *β at elevated temperature and the thermodynamic parameters $\Delta_R H°_m$ and $\Delta_R S°_m$*

Determination of the Conditional Constants at Elevated Temperature

To determine the molality of the free $H_3PO_4$ for the slope analysis at elevated temperature, the $H^+$ molality was assumed to be constant from 25 to 90 °C during the speciation calculations. Indeed, pH measurements up to 80 °C performed in our former study [16] did not reveal significant differences from the $pH_{exp}$ values recorded at 25 °C.

Following the same methodology described above, the terms $\log_{10}\frac{m_{Cm(H_2PO_4)^{2+}}}{m_{Cm^{3+}}} + \log_{10} m_{H^+}$ and $\log_{10}\frac{m_{Cm(H_2PO_4)_2^{+}}}{m_{Cm^{3+}}} + 2\log_{10} m_{H^+}$ were plotted as a function of $\log_{10} m_{H_3PO_4}$ at an ionic strength of 1 mol·L$^{-1}$ and at 40, 50, 60, 80, and 90 °C (see Figure S6 in SI for $Cm(H_2PO_4)^{2+}$ and Figure S7 in SI for $Cm(H_2PO_4)_2^{+}$). All slopes were close to one for $Cm(H_2PO_4)^{2+}$ and close to two for $Cm(H_2PO_4)_2^{+}$, indicating no change in the stoichiometry of the formed complexes upon increasing temperature. All resulting conditional $\log_{10}$ *β values for $Cm(H_2PO_4)^{2+}$ and $Cm(H_2PO_4)_2^{+}$ as well as their uncertainties are reported in Table 5 and Table 6.

Upon increasing the temperature, both equilibria $Cm^{3+} + H_3PO_4 \rightleftharpoons Cm(H_2PO_4)^{2+} + H^+$ and $Cm^{3+} + 2\ H_3PO_4 \rightleftharpoons Cm(H_2PO_4)_2^{+} + 2\ H^+$ were shifted towards the product side, revealing an increase in the conditional complexation constants, as already visible in the luminescence data discussed in the previous section.

Table 5:. Thermodynamic conditional (I = 1.1 mol·L$^{-1}$ at $-\log_{10}[H^+] = 1.00$ and I = 1.0 mol·L$^{-1}$ at $-\log_{10}[H^+] = 2.52$) and extrapolated to infinite dilution complexation constants for the formation of $Cm(H_2PO_4)^{2+}$ at elevated temperature ($\log_{10}$ *β in the molal scale).

| Temperature (°C) | Ionic strength (mol·L$^{-1}$) | $-\log_{10}[H^+]$ | $\log_{10}$ *$\beta_1$ | $\log_{10}$ *$\beta_1$° |
|---|---|---|---|---|
| 40 | 1.1 | 1.00 | −0.12 ± 0.10[a] | 0.53 ± 0.10[b] |
| 50 | 1.1 | 1.00 | −0.08 ± 0.20[a] | 0.59 ± 0.20[b] |
| 60 | 1.1 | 1.00 | −0.02 ± 0.10[a] | 0.67 ± 0.10[b] |
| 80 | 1.1 | 1.00 | 0.02 ± 0.10[a] | 0.75 ± 0.10[b] |
| 40 | 1.0 | 2.52 | −0.08 ± 0.10 | 0.58 ± 0.10 |
| 50 | 1.0 | 2.52 | −0.03 ± 0.10 | 0.64 ± 0.10 |
| 60 | 1.0 | 2.52 | 0.01 ± 0.10 | 0.70 ± 0.10 |
| 80 | 1.0 | 2.52 | 0.15 ± 0.10 | 0.88 ± 0.10 |
| 90 | 1.0 | 2.52 | 0.19 ± 0.10 | 0.95 ± 0.10 |

[a] Values were taken from Jordan et al. (2018)[16]
[b] Uncertainties were recalculated based on the ion interaction coefficient derived in this study

Table 6. Thermodynamic conditional (I = 1.0 mol·L$^{-1}$ at –log$_{10}$ [H$^+$] = 2.52) and extrapolated to infinite dilution complexation constants for the formation of $Cm(H_2PO_4)_2^+$ at elevated temperature (log$_{10}$ *β in the molal scale).

| Temperature (°C) | log$_{10}$ *β$_2$ | log$_{10}$ *β$_2$° |
|---|---|---|
| 40 | −0.78 ± 0.20 | 0.16 ± 0.20 |
| 50 | −0.64 ± 0.20 | 0.33 ± 0.20 |
| 60 | −0.56 ± 0.20 | 0.44 ± 0.20 |
| 80 | −0.38 ± 0.20 | 0.68 ± 0.20 |
| 90 | −0.24 ± 0.20 | 0.85 ± 0.20 |

The highest uncertainty for the average log$_{10}$ *β reported in Table 5 and Table 6 was not exceeding 0.02. The same approach described in section 2.1.2 was applied to reach the final uncertainties reported in Table 5 and Table 6.

Extrapolation to infinite dilution

Similarly to the approach used at 25 °C, the conditional complexation constants were extrapolated to infinite dilution applying the SIT equation. At 40 °C (A = 0.523 kg$^{1/2}$·mol$^{-1/2}$) and 50 °C (A = 0.534 kg$^{1/2}$·mol$^{-1/2}$), the Debye–Hückel term was taken from the values tabulated by Lemire et al. (2020).[23] At 60, 80, and 90 °C, they were calculated according to Moog and Voigt (2011)[29] and were found to be 0.546, 0.571, and 0.585 kg$^{1/2}$·mol$^{-1/2}$, respectively.

For the extrapolation to infinite dilution, the ion interaction coefficients derived at 25 °C were assumed to be constant in the temperature range from 25 to 90 °C, according to Lemire et al. (2020)[23] who reported a very small temperature dependency of the ion interaction coefficients between 25 and 200 °C (with $(\partial\varepsilon/\partial T)_p < 0.005$ kg·mol$^{-1}$·K$^{-1}$ at T < 200 °C). The obtained log$_{10}$ *β° values at 40, 50, 60, 80, and 90 °C for $Cm(H_2PO_4)^{2+}$ and $Cm(H_2PO_4)_2^+$ are summarized in Table 5 and Table 6. The uncertainties on log$_{10}$ *β°(T) were obtained from the uncertainties on log$_{10}$ *β(T) and Δε as follows:

$$\sigma_{\log_{10}{}^*\beta^0} = \sqrt{\sigma^2_{\log_{10}{}^*\beta} + (m_{ClO_4^-} \cdot \sigma_{\Delta\varepsilon})^2} \qquad \text{(Eq. 12)}$$

Note that the conditional complexation constants at elevated temperatures taken form Jordan et al. (2018)[16] were extrapolated to infinite dilution using the ion interaction coefficients determined in the present study.

Derivation of thermodynamic data

The standard molal enthalpy of reaction $\Delta_R H_m^0$ and standard molal entropy of reaction $\Delta_R S_m^0$ were obtained using the integrated van't Hoff equation (Eq. 13), assuming $\Delta_R S_m^0$ value to remain constant between 25 and 90 °C. The same assumption was done for the molal enthalpy of reaction, assuming the molal standard heat capacity of reaction $\Delta_R C_{p,m}^0$ to be constant and equal to zero.

$$\log_{10} K^0(T) = \log_{10} K^0(T_0) + \frac{\Delta_r H^0(T_0)}{R \ln 10}\left(\frac{1}{T_0} - \frac{1}{T}\right) \qquad \text{(Eq. 13)}$$

R being the universal molar gas constant (8.314 $J \cdot K^{-1} \cdot mol^{-1}$) and T the temperature in Kelvin ($T_0$ = 298.15 K).

Results are shown in Figure 5 and explanations about the weighted least squares regression were already mentioned in section 2.1.2.

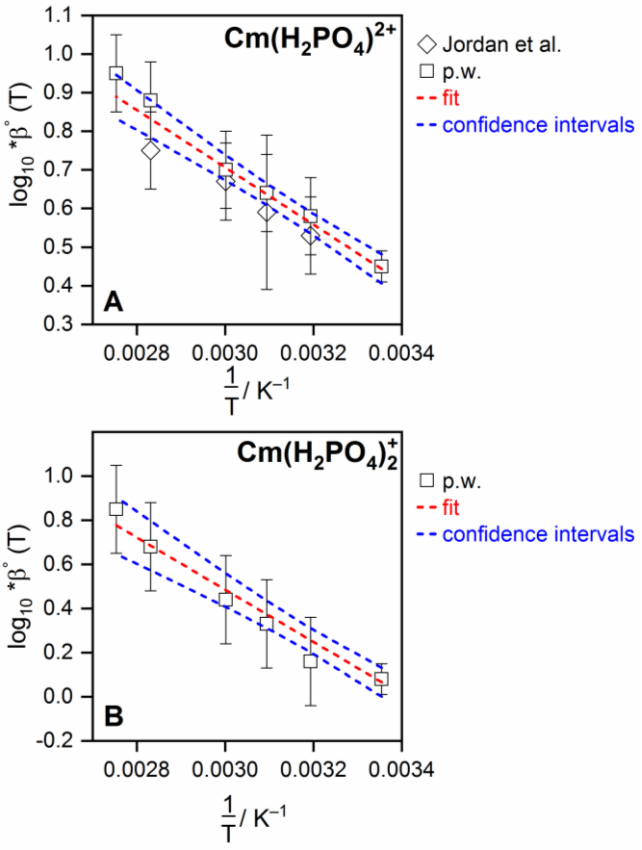


Figure 5: van't Hoff plots for the $Cm(H_2PO_4)^{2+}$ (A) and $Cm(H_2PO_4)_2^{+}$ (B) complexes, based on the data in Table 5 and Table 6.

The derived thermodynamic data are summarized in Table 7 together with the corresponding weighted sum of squared residuals (WSOSR).

Table 7. Thermodynamic data derived for the $Cm(H_2PO_4)^{2+}$ and $Cm(H_2PO_4)_2^{+}$ complexes using the integrated van't Hoff equation.

| Thermodynamic data | $Cm^{3+} + H_3PO_4 \rightleftharpoons Cm(H_2PO_4)^{2+} + H^+$ | $Cm^{3+} + 2\ H_3PO_4 \rightleftharpoons Cm(H_2PO_4)_2^{+} + 2\ H^+$ |
|---|---|---|
| $\Delta_R H_m^0$ (kJ·mol$^{-1}$) | 14.2 ± 1.1 | 22.7 ± 1.8 |
| $\Delta_R S_m^0$ (J·mol$^{-1}$·K$^{-1}$) | 56.1 ± 3.3 | 77.3 ± 5.7 |
| WSOSR | 1.612 | 0.499 |

All thermodynamic data for both complexes were found to be positive, meaning that the reactions were endothermic and entropy–driven. The temperature dependent complexation constants were also described with the extended van't Hoff equation (see Supporting Information). Interestingly, for the $Cm(H_2PO_4)^{2+}$ complex, considering in addition the standard molal heat capacity of reaction does not significantly improve the WSOSR (1.612 vs. 1.327) of the fit and delivers a $\Delta_R C_{p,m}^0$ value with a large uncertainty (cf. Table S1 in SI). The situation for the $Cm(H_2PO_4)_2^{+}$ complex is different. There, the WSOSR of the fit is improved by almost one order of magnitude (0.499 vs. 0.073), which allows a better description of the data.

## 2.3 Cm(III) complex structures and coordination

### *2.3.1 Ab initio calculations*

All the Cm(III) complexes with one or two dihydrogenphosphate ligands are found to be monodentate complexes in the solvated phase. By comparison, the Gibbs free energy of $[Cm(H_2O)_8H_2PO_4]^{2+}$ with exclusive monodentate bonds between the $H_2PO_4^-$ ligand and the curium, is lower by 10 kJ·mol$^{-1}$ compared to the one for which the curium formed a double bond with the $H_2PO_4^-$ ligand. A tendency which is inversed in gas–phase. The considered complexes are represented in Figure 6.

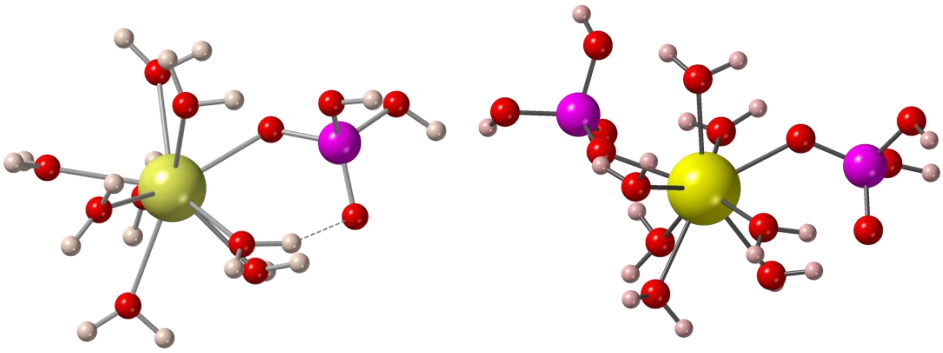

Figure 6: Complexes of $[Cm(H_2O)_8H_2PO_4]^{2+}$ (left) and $[Cm(H_2O)_7(H_2PO_4)_2]^{+}$ (right) optimized at the ump2 level of theory (Cm are in yellow, O in red, H in white, P in violet). Dashed line = hydrogen bond.

In the 1:1 complexes, the monodentate dihydrogenphosphate binds Cm at a very short distance of 2.260 and 2.297 Å for the 8 and 9–coordinated complexes, respectively, while all Cm–$OH_2$ distances, except for a long one at 2.57 Å, lie between 2.44 and 2.53 Å, i.e. in the range of those computed for the Cm aquo ion (Table S2 in SI). For the 1:2 complexes, the distances to the monodendate oxygen atoms of the two dihydrogenphosphate groups appear to be longer by 0.05 Å for CN = 8 and 0.07 Å for CN = 9 than in the 1:1: complexes, because of their mutual steric repulsion (Table S2 in SI). The very short distance between Cm and the interacting oxygen of the dihydrogenphosphate group plus the anionic character of the ligand may suggest that the character of this bond is different from that between Cm and a neutral water molecule. However, as observed in Table S3 in SI, the QTAIM analysis that compares the $Cm(H_2PO_4)^{2+}$ complex to the aquo complex shows that the $Cm - O_{H_2PO_4}$ bond is about the same type than the typical $Cm - O_{H_2O}$ bond, that is essentially ionic, similar to other *An* or *Ln* ions interacting with inorganic or organic ligands.[30-32]

The exploration of the relative stability of hydrated species is also possible owing to the estimation of the Gibbs free energy of reactions $\Delta G_r(T)$, as defined in the section 5.4.3. For the reaction (R–3) involving exclusively the aquo ion, $\Delta G_r$ = +6 kJ·mol$^{-1}$ at 25 °C and +0.7 kJ·mol$^{-1}$ at 90 °C were computed, i.e. a constant number of coordination of nine is favored at 25 °C (about 90%). Albeit at 90 °C the population of 8 coordinated aquo ion increases, the coordination is still dominated by the nine–coordinated one. This result is fully consistent with the Gibbs free energy value $\Delta G_r$ = +5.5 kJ·mol$^{-1}$, estimated by Lindqvist–Reis et al. (2005).[33] For the 1:1 complexes, the computed Gibbs free energy of reaction for the reaction (R–4) corresponding to the water dissociation process from the nine–coordinated $[Cm(H_2O)_8(H_2PO_4)]^{2+}$ is endergonic, $\Delta G_r$ = +2.3 kJ·mol$^{-1}$, suggesting that the solution might contain a large amount of nine–coordinated species. For the 1:2 complexes, the $\Delta G_r$ associated to the reaction (R–5), is estimated to be at −7.5 kJ·mol$^{-1}$ at 25 °C, meaning that one

would possibly expect a decrease of the coordination number from 9 to 8, a tendency reinforced by the raise of the temperature ($\Delta G_r = -13.9$ kJ·mol$^{-1}$ at 90 °C).

However, one has to be aware that we are reaching here a certain limit of the QM methods at predicting accurately thermodynamic properties.

Based on the optimized Cm(III)–complex structures, the *ab initio* absorption/emission wavelengths of five considered $[Cm(H_2O)_n(H_2PO_4)_m]^{(3-m)+}$ complexes are reported, with n + m = 8 or 9 and n varying from 6 to 9. The data are available in Table S4 in SI for a coordination number equal to 9 and Table S5 in SI for CN = 8. They are associated to absorption energies averaged over the 8 spin–orbit components of the spin–free octet ground state to the lowest components of the sextet states. The absolute absorption energies are corrected by an estimated shift $\Delta E_{XMS-CASPT2}$ (as defined in section 5.4.2).

For the $[Cm(H_2O)_9]^{3+}$ complex, geometry optimizations at the CASSCF level for the octet ground state and the lowest sextet state were carried out and it turned out that the changes in the Cm–$OH_2$ distances did not exceed a few picometers. This leads to the conclusion that one can compute emission energies and wavelengths using the ground–state octet geometry. Note that the resulting absolute absorption/emission energies might be slightly shifted with respect to experimental data, as the chemical model and the method used to optimize the geometries might impact them; computed first–shell distances might be about 0.50 Å too long.[32, 34] However, as shown in recent computational studies of Ce(III) spectroscopy,[32, 35] one can expect the computed quantities to be accurate enough to discuss trends in emission energies with respect to changes in either the coordination number or the first–coordination shell ligand.

According to the quantum chemical calculations, the complexation of Cm with one or two hydrogen phosphate group(s) results in a small lowering of the emission energies by only few hundreds cm$^{-1}$ compared to the aquo ion, thus corresponding to a small red shift. This theoretical result is perfectly in line with the experimental observations (see section 2.1.1) as well as our former study,[16] even though the computed redshift is slightly overestimated, as expected regarding the "computational" constraints.

For the sake of the comparison with luminescence spectroscopic data acquisition, an additional and interesting feature that can be deduced from the simulations, is the crystal field splitting (CFS) of the low–lying excited states of the complexes. Here, we specifically mean the few lowest components of the sextet states which are within 1000 cm$^{-1}$ of the lowest one. In the 1:1 complex for CN = 9, the computed splitting $\Delta E(A_4-A_1)$ of 432 cm$^{-1}$ is slightly

larger than the one in the 1:2 complex, i.e. 378 $cm^{-1}$, both being larger than what was found for the $[Cm(H_2O)_9]^{3+}$ aquo ion, i.e., 273 $cm^{-1}$ (Table S4 in SI). Note that the reduction of the first–coordination sphere by one water molecule results in an increase of the crystal–field splitting by a factor of 1.3 for the aquo ion and 1:1 complex, and a factor of 1.5 for the 1:2 complex (see Tables S4 and S5 in SI, ratio $\Delta E(B_4-B_1) / \Delta E(A_4-A_1)$).

*2.3.2 Luminescence spectroscopy*

In order to assess the complex structures in more detail and to account for potential changes in the overall coordination number with increasing temperature, the spectroscopic data in terms of obtained pure component spectra can be compared with the computed data for the Cm(III) electronic levels in the different complex coordinations (8–fold vs. 9–fold).

From the obtained pure component spectra, the CFS can be determined when the emission profiles are fitted with four Lorentzian functions. The prerequisite for the fitting is that the population of these crystal field states follows the Boltzmann distribution (Eq. 16). The obtained peak positions of the four Lorentzian peaks can thereafter be compared to the computed crystal field splitting for the two identified Cm–phosphate complexes with overall coordination numbers of 8 or 9.

For such comparison, one has to begin the discussion with the non–complexed $Cm^{3+}$ aquo ion. At 25 °C, more than 90% of the aquo ion has been shown to exist in solution as the nine–hydrated tricapped–trigonal–prismatic $Cm(H_2O)_9^{3+}$ cation.[33] The remaining ~ 10% is 8–fold coordinated $Cm(H_2O)_8^{3+}$ with a square–antiprismatic structure. With increasing temperature, the amount of 8–fold coordinated $Cm^{3+}$ ions increases, so that at 90 °C (the highest temperature used in the present study) approximately 20% of the $Cm^{3+}$ aquo ion has 8–fold coordination. The presence of both 8–fold and 9–fold coordinated Cm(III) can be directly observed in the measured Cm(III) aquo ion emission spectrum as a shoulder on the red side of the emission peak (see Figure S9 in SI). The emission spectrum collected at 90 °C has been fitted with two approaches: i) considering both coordinations of the aquo complex by fitting the main transitions ($A_1$) of both $Cm(H_2O)_9^{3+}$ and $Cm(H_2O)_8^{3+}$ and three composite hot–band transitions describing the 6 crystal fields states ($A_2$–$A_4$) of the two aquo ion configurations, and ii) only considering the presence of 9–fold coordinated aquo ion with an overall of four crystal field transitions. The latter fit is clearly unsatisfactory, highlighting the visible presence of a significant amount of $Cm(H_2O)_8^{3+}$ in the measured emission spectrum collected at this elevated temperature. Further discussion of the obtained fit and resulting crystal field splitting in comparison to the computed one is given in the SI (see text and Table S6 in SI).

To explore the possibility of a change in coordination for the two extracted Cm(III)–phosphate complexes with increasing temperature, the extracted pure component spectra were analyzed in detail. We begin the discussion with the 1:1 $Cm(H_2PO_4)^{2+}$ complex. The extracted pure component emission spectra for this Cm–phosphate complex at 25 °C and 90 °C were fitted with four Lorentzian peaks (emission transition from the crystal field levels $A_1$–$A_4$ back to the ground state) following the Boltzmann distribution. This fit assumes that only one complex configuration (*e.g.*, only 8–fold or only 9–fold coordination) is present in solution at both temperatures. As illustrated in Figure 7, this fit reproduced the experimental data very well. No deviation on the red side of the spectrum (indicated in Figure 7 with an arrow), which would point toward the presence of an additional complex configuration as observed for the Cm(III) aquo ion, can be observed. The largest deviation from the extracted pure component emission spectrum can be seen at 25 °C around 585 nm, which can be related to the rather large error of the fitted peak position of the crystal field transition $A_4$ (errors for the Lorentzian peak centers are included in the plots in Figure 7). With increasing temperature, the population of the crystal field levels increases and the error associated with the Lorentzian fits of these hot–band transitions decreases. All fitted parameters with associated errors are compiled in the SI, Table S7.

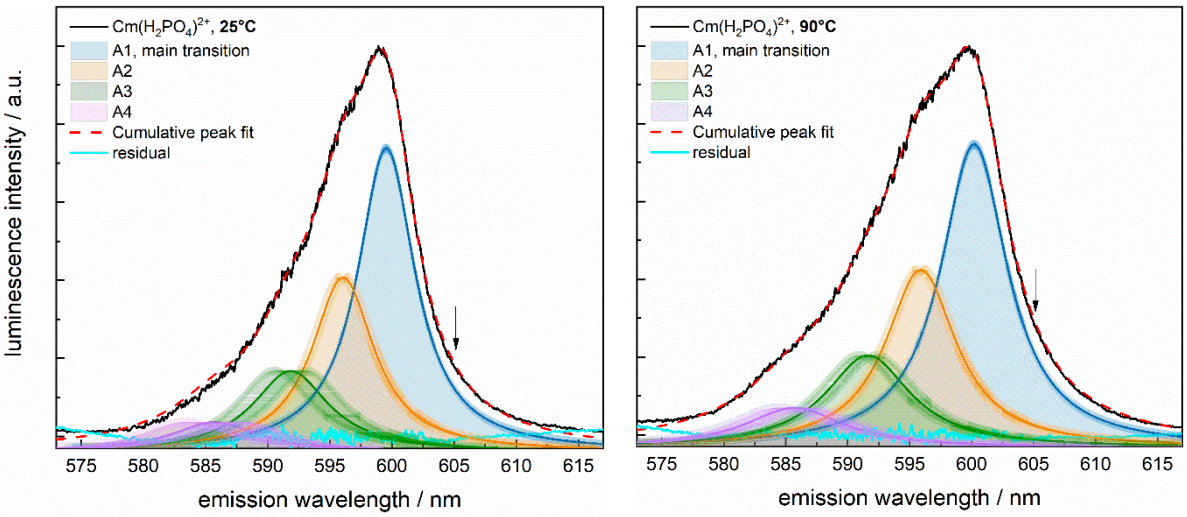


Figure 7: Extracted pure component emission spectra (black curves) of the $Cm(H_2PO_4)^{2+}$ complex at 25°C (left) and 90 °C (right) can be described with four Lorentzian peaks following the Boltzmann distribution depicting the emission transitions from the four crystal field states of the excited electronic level ($A_1$–$A_4$) back to the ground state. Errors expressed with 99.7% (3σ) confidence of the fitted Lorentzian peak maxima and the fit residual (cyan traces) are included in the plots. Arrows indicate the part of the spectrum where the presence of an 8–fold coordinated $Cm(H_2PO_4)^{2+}$ complex would be expected to appear.

At 90 °C the composite spectrum as well as the fitted Lorentzian functions of the $Cm(H_2PO_4)^{2+}$ complex are broader than at 25 °C, owing to inhomogeneous broadening of the spectral lines with increasing temperature.[36] From the obtained peak maxima of the

Lorentzian peaks, representative of the energy of the crystal field transitions, the magnitude of the crystal field splitting can be calculated. The results are compiled in Table 8 together with the computed crystal field splitting for the Cm(III)–phosphate complex in 8–fold and 9–fold coordination. The magnitude of the crystal field splitting at the two investigated temperatures is very similar, yielding average values of 0 ($A_1$), 107 ($A_2$–$A_1$), 224 ($A_3$–$A_1$), and 380 ($A_4$–$A_1$). This splitting is in excellent agreement with the computed crystal field splitting for the $Cm(H_2PO_4)^{2+}$ complex with an overall coordination number of 9, see Table 8. Therefore, this Cm(III)–phosphate complex can with confidence be assigned to the 9–fold coordinated $Cm(H_2O)_8(H_2PO_4)^{2+}$ species. Based on the identical crystal field splitting at 25 °C and 90 °C and the absence of any features in the extracted pure component emission spectra which cannot be described using the four Lorentzian peaks, this coordination is preserved over the entire investigated temperature range. In other words, a similar decrease of the coordination number from 9 to 8 as observed for the curium aquo ion as a function of temperature does not occur for this phosphate complex.

Table 8: The crystal field splitting (CFS) obtained from the fitted experimental pure component emission spectra for the $Cm(H_2PO_4)^{2+}$ and $Cm(H_2PO_4)_2^{+}$ complexes are compared with the computed CFS for these complexes in 8–fold and 9–fold coordination.

| Crystal field splitting of the 1:1 $Cm(H_2PO_4)^{2+}$ complex | | | | | | | |
|---|---|---|---|---|---|---|---|
| Exp. CFS 25 °C | Exp. CFS 90 °C | Comp. CFS CN = 9 | ΔCFS 25 °C (comp.–exp.) CN = 9 | ΔCFS 90 °C (comp.–exp.), CN = 9 | Comp. CFS CN = 8 | ΔCFS 25 °C (comp.–exp.) CN = 8 | ΔCFS 90 °C (comp.–exp.), CN = 8 |
| 0 | 0 | 0 | 0 | 0 | 0 | 0 | 0 |
| 98 ± 8.5 | 117 ± 7.1 | 112 | 14 | –5 | 165 | 67 | 48 |
| 217 ± 36 | 233 ± 19 | 291 | 74 | 58 | 303 | 86 | 70 |
| 364 ± 70 | 396 ± 35 | 432 | 68 | 36 | 565 | 201 | 169 |
| Crystal field splitting of the 1:2 $Cm(H_2PO_4)_2^{+}$ complex | | | | | | | |
| 0 | 0 | 0 | 0 | 0 | 0 | 0 | 0 |
| 170 ± 24 | 162 ± 6.0 | 128 | –42 | –34 | 141 | –29 | –21 |
| 301 ± 68 | 262 ± 21 | 229 | –72 | –33 | 241 | –60 | –21 |
| 451 ± 63 | 437 ± 54 | 378 | –73 | –59 | 573 | 122 | 136 |

A similar treatment of the pure component spectra for the $Cm(H_2PO_4)_2^+$ complex was done to obtain the crystal field splitting at 25 °C and 90 °C. The obtained results for these two temperatures are shown below in Figure 8. The experimental and computational data of the crystal field splitting are compiled in Table 8, while a compilation of all fitting parameters can be found in Table S8.

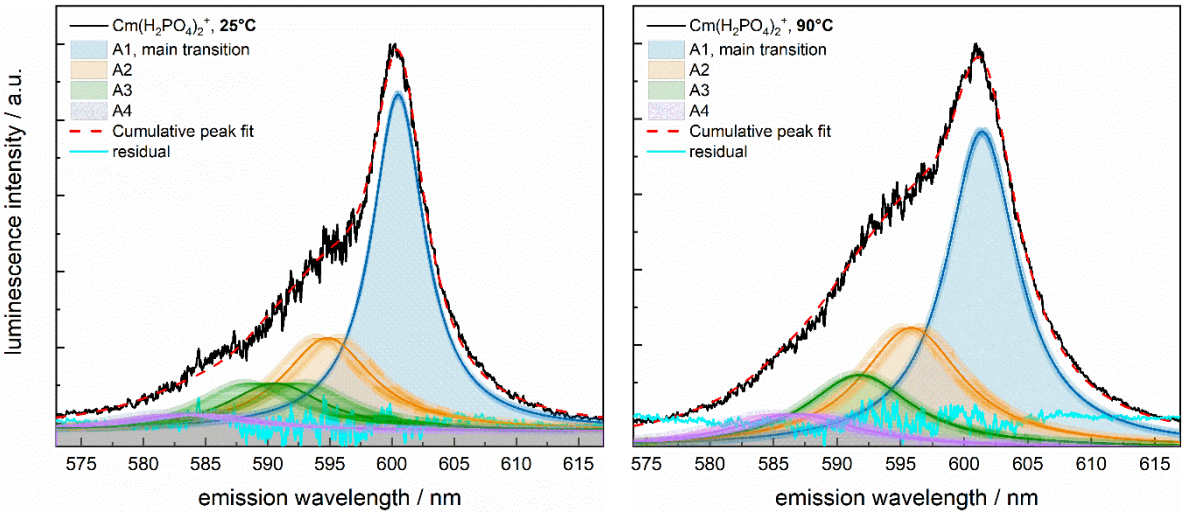


Figure 8: Extracted pure component emission spectra (black curves) of the $Cm(H_2PO_4)_2^+$ complex at 25°C (left) and 90 °C (right) can be described with four Lorentzian peaks following the Boltzmann distribution depicting the emission transitions from the four crystal field states of the excited electronic level ($A_1$–$A_4$) back to the ground state. Errors expressed with 99.7% (3σ) confidence of the fitted Lorentzian peak maxima and the fit residual (cyan traces) are included in the plots.

In contrast to the 1:1 species where the computed crystal field splitting for the 8–fold and 9–fold coordinated $Cm(H_2PO_4)^{2+}$ complex are clearly different, a very similar splitting is obtained for both coordinations of the $Cm(H_2PO_4)_2^+$ complex, see Table 8. The largest difference can be seen for the $A_4$–$A_1$ band gap, which unfortunately inherits the largest error in the fitted experimental profiles due to the low population of the highest crystal field level, especially at 25 °C. When omitting this level from the comparison, a better fit with the computed data for the 8–fold coordinated complex can be deduced. If the $A_4$ level is included, the 9–fold coordinated species seems to yield the most consistent result, which is in agreement with the coordination of the 1:1 complex. Therefore, a direct conclusion of the coordination of this species is hard to draw.

In comparison to the fitted profiles of the 1:1 complex, the fitting residual of the 1:2 complex (cyan traces in Figure 8) is larger. The worse fit of the latter complex is also visible from the SOSR values (compiled for all fits in Table S9 in SI) which is larger by a factor of 2 at 25 °C and by a factor of almost 4 at 90 °C in comparison to the values obtained for the 1:1 complex.

As our computational results point toward a possible presence of 8–fold coordinated $Cm(H_2PO_4)_2^+$, the fit was redone with addition of a fifth Lorentzian function describing the $A_1$ transition of such an 8–fold coordinated complex configuration (similarly to the procedure described above for the aquo ion). To facilitate the interpretation of the results, pure component spectra for the 1:2 complex collected at 40, 60, and 80 °C were included in the data treatment. The results for all five temperatures are compiled in Figure S10 and Table S10 in SI. At 25 and 40 °C, the fits are not improved by the inclusion of this fifth Lorentzian component depicting the presence of $Cm(H_2PO_4)_2^+$ with CN = 8 (see Table S9 in SI). At 60–90 °C, however, the SOSR become systematically better with five components rather than four, which serves as an indication for the presence of 8–fold coordinated $Cm(H_2O)_6(H_2PO_4)_2^+$ in addition to $Cm(H_2O)_7(H_2PO_4)_2^+$ in 9–fold coordination. Based on the area under the curves of the main transition ($A_1$) peaks, the amount of the 8–fold coordinated species increases from 2% at 25 °C to 14% at 90 °C. However, as the individual hot–band transitions of both coordinations cannot be resolved and hot–bands of the 8–fold coordinated complex can be expected to overlap with the main transition of the 9–fold coordinated species, these values should be taken as tentative, yielding information of the trends in the system rather than the absolute speciation.

## 3 Discussion

Based on our luminescence spectroscopic data, three different Cm(III)–phosphate complexes could be derived from our peak deconvolution. Only two complexes could be identified in solution at the lower investigated pH value of $-\log_{10}[H^+] = 2.52$. Based on slope analysis of the derived species distributions, these two species could be assigned to $Cm(H_2PO_4)^{2+}$ and $Cm(H_2PO_4)_2^+$ with complexation constants at infinite dilution of $\log_{10} {}^*\beta^0 = 0.45 \pm 0.04$ (reaction R–1) and $\log_{10} {}^*\beta^0 = 0.08 \pm 0.07$ (reaction R–2), respectively. Recalculating these values for the reactions $Cm^{3+} + H_2PO_4^- \rightleftharpoons Cm(H_2PO_4)^{2+}$ and $Cm^{3+} + 2\ H_2PO_4^- \rightleftharpoons Cm(H_2PO_4)_2^+$ using the reaction $H^+ + H_2PO_4^- \rightleftharpoons H_3PO_4$ ($\log_{10} \beta° = 2.14 \pm 0.03$)[23] yields complexation constants of $\log_{10} \beta^0 = 2.59 \pm 0.05$ and $\log_{10} \beta^0 = 4.36 \pm 0.09$. The complexation constant for the 1:1 complex is identical to the one derived in our previous study ($2.59 \pm 0.19$),[16] however, due to the larger amount of data points used for the extrapolation and recalculation of the complexation constant and the slightly different statistical approach in the present work, the uncertainty is substantially smaller. The confirmation of a complex stoichiometry of 1:2 for the second Cm(III)–phosphate complex is rather surprising as the two

most recent studies compiled in Table 1, accounting for more than one *An*–phosphate complex, only report on $An(H_2PO_4)^{2+}$ and $An(HPO_4)^{+}$ species (*An* = Am or Cm).[17, 20] In both the studies of Moskvin (1969) [19] and Lebedev et al. (1979),[22] however, the formation of 1:2 $An(H_2PO_4)_2^{+}$ complexes have been proposed. In the latter study, slope analysis of the spectrophotometric data yielded a complexation constant of 3.72 ± 0.02 for $Am(H_2PO_4)_2^{+}$, a value which is substantially lower than the corresponding one for the $Cm(H_2PO_4)_2^{+}$ complex reported in the present study. Lebedev et al. (1979),[22] however, worked at very high total phosphate concentrations (up to 13 $mol \cdot L^{-1}$) and the ionic strength was not kept constant in their study. Therefore, this complex and the postulated complexation constant were not accepted by Silva et al. (1995)[24] with the explanation that the experimental conditions in terms of the very high ionic strength could lead to ionic strength artefacts such as the decrease of the molar extinction coefficient in the quasi "non–aqueous" media. Thus, our study is the first one to report a complexation constant for the 1:2 complex under controlled ionic strength conditions.

The interaction coefficient $\varepsilon(Cm(H_2PO_4)^{2+};ClO_4^{-})$ (0.17 ± 0.04 $kg \cdot mol^{-1}$) was found to be larger than $\varepsilon(Cm(H_2PO_4)_2^{+};ClO_4^{-})$ (−0.10 ± 0.06 $kg \cdot mol^{-1}$), which can be attributed to the higher charge density of the $Cm(H_2PO_4)^{2+}$ complex. This is in line with the computed bond length between Cm and the oxygen atoms of the dihydrogenphosphate ligand, which is shorter in the $Cm(H_2PO_4)^{2+}$ complex (see section 2.3.1).

As the temperature increases from 25 to 90 °C, the relative permittivity of water, or more commonly called dielectric constant $\varepsilon_r$, decreases from 78 to 58, due to an increased thermal agitation in the system, leading to an increased entropy coming from an increased disorder. This, combined with the release of one or two $H_2O$ molecules from the first coordination shell of the aquo ion upon complexation of the $H_2PO_4^{-}$ ligand(s), contributes to the overall increase in the entropy, in agreement with the positive $\Delta_R S_m^0$ values derived from the application of the integrated van't Hoff equation to the temperature dependent data.

Based on our *ab initio* calculations, both the 1:1 and 1:2 Cm–phosphate complexes with monodentate coordination to the $H_2PO_4^{-}$ ligand are the most stable complex configurations at 25°C. This coordination is supported by our luminescence lifetime measurements, where a very small increase of the overall luminescence lifetime was observed with increasing phosphate complexation. As previously mentioned, the lifetimes could be well described by the coordination of 8 or 7 $H_2O$ entities to the curium cation in the $Cm(H_2PO_4)^{2+}$ and $Cm(H_2PO_4)_2^{+}$ complexes, respectively, using Eq. 1, proposed by Kimura and Choppin.[26]

When preserving an overall Cm(III) coordination number of 9, only monodentate coordination to the $H_2PO_4^-$ ligand is possible.

At elevated temperature, however, our *ab initio* simulations predict a different behavior in terms of the coordination, for the two identified Cm(III)–phosphate complexes. For the $Cm(H_2PO_4)^{2+}$ species, the coordination number is predominantly 9 both at 25 and 90 °C, which is in agreement with the deconvolution and subsequent Boltzmann fitting of the luminescence emission spectra (see section 2.3.2). However, for the $Cm(H_2PO_4)_2^+$ complex, a decrease of the coordination number from 9 to 8 could be favored. The steric repulsion due to the presence of two dihydrogenphosphate groups together with a reduced charged density, leading to an increased length of some of the $Cm - O_{H_2O}$ bonds becoming then more labile, could explain this behavior. Note that the coordination number of 8 in the $Cm(H_2PO_4)_2^+$ complex implies a higher symmetry, also related to an increased disorder. In addition, both *ab initio* simulations (see section 2.3.1) and deconvolution of the luminescence spectra (see section 2.3.2) revealed an increased amount of 8–fold coordinated $Cm^{3+}$ ion with temperature (≈ 14% at 90 °C). The decrease of the coordination number of the Cm(III) aquo ion as a function of temperature was found to be entropy driven ($\Delta S = 25.4 \pm 1.2$ J·mol$^{-1}$·K$^{-1}$).[33] This could also be a driving force to the decreased coordination number for the 1:2 $Cm(H_2PO_4)_2^+$ complex.

The unfavorable enthalpy of reaction observed for both Cm–phosphate complexes reveals that the heat spent in the loss of water molecules is not regained upon the interaction of the $H_2PO_4^-$ ligand(s) with the $Cm^{3+}$ ion. Interestingly, the temperature–dependent complexation data of the $Cm(H_2PO_4)^{2+}$ complex is well described using the integrated van't Hoff equation. For the $Cm(H_2PO_4)_2^+$ complex, the fit was improved by one order of magnitude when the extended van't Hoff equation was applied. Both integrated and extended van't Hoff equations possess two fit parameters, therefore the decreased WSOSR for the extended van't Hoff equation is not due to the presence of a different number of variables to be fitted.

This could be the result of the presence of two $Cm(H_2O)_7(H_2PO_4)_2^+$ and $Cm(H_2O)_6(H_2PO_4)_2^+$ species being 9–fold and 8–fold coordinated, respectively, with temperature dependent fractions (see section 2.3.2). This would imply that the "single pure" component spectrum derived from the luminescence data for the 1:2 complex would in fact correspond to a mixture of 8–fold and 9–fold coordinated species. The same is true for the $Cm^{3+}$ aquo ion (see section 2.3.2). Ideally, one should extract the relative distribution of $Cm^{3+}$ and $Cm(H_2PO_4)_2^+$ with CN = 8 and CN = 9 during the deconvolution of the luminescence spectra. However, this is not

possible as the increase of temperature does not only lead to an increase of the 8–fold coordinated species but also to an increase of the hot–band intensities of both the 9–fold and 8–fold coordinated species. Therefore, a difference spectrum aiming at extracting the emission spectrum of $Cm(H_2O)_6^+(H_2PO_4)_2$ would show additional peaks belonging to the hot–band transitions of the $Cm(H_2O)_7^+(H_2PO_4)_2$ complex. With individual components it would be conceivable to apply the SIT theory for two species with different coordination numbers if their relative proportion is known, and to derive for each of them a complexation constant at infinite dilution together with an ion interaction coefficient. Subsequently, the integrated van't Hoff equation could be applied to obtain enthalpies and entropies of reaction for the 8– and 9–fold coordinated species. Eventually, the derived complexation constants at infinite dilution taking into account changes in the coordination number could be implemented in thermodynamic databases, by including the water molecules in the first hydration shell of the ions/complexes. Common geochemical speciation software can already handle water molecules in chemical reactions in which they get deprotonated (e.g. hydrolysis reactions) or for solubility products of solid phases containing water of hydration. Including the water molecules in the first hydration shell of ions/complexes is currently not possible and would require further code developments.

The decrease of the coordination number upon increasing temperature could not only apply to the Cm–phosphate system, but as well to complexation studies with other inorganic ligands such as nitrate, sulfate, hydroxide, etc. This phenomenon is unfortunately simply overlooked in almost all complexation studies. Our results indicate that this aspect should be systematically examined, in particular when it comes to chemical species with more than one ligand in their first coordination sphere, which was shown to favor a decrease in the coordination number for the Cm(III)–phosphate system at elevated temperatures.

When increasing the pH to $-\log_{10}[H^+] = 3.44 - 3.65$, the presence of a third Cm(III)–phosphate complex could be observed in the current study. Due to the overall low amount of this species, however, a reliable slope analysis could not be performed and we can only tentatively assign this species to the $Cm(HPO_4)^+$ complex identified in the studies by Rao et al. (1986)[20] and Moll et al. (2011).[17] At the chosen solution conditions in the present work, we are very close to the solubility limit of solid $CmPO_4{\cdot}xH_2O$ based on existing solubility data for amorphous $AmPO_4{\cdot}xH_2O$ [37] and crystalline $LnPO_4{\cdot}0.667H_2O$ rhabdophane.[38] Therefore, finding suitable solution conditions where an adequate amount of the $Cm(HPO_4)^+$ complex is present in solution while avoiding Cm–phosphate precipitation, will be challenging even with such a sensitive spectroscopic method as luminescence spectroscopy allowing for the

detection of sub–nanomolar Cm(III) concentrations. Alternatively, solid $CmPO_4 \cdot xH_2O$ could be deliberately precipitated from solution and characterized with luminescence spectroscopy, in order to determine a luminescence emission spectrum for this colloidal species. This would allow for analysis of suspensions where both such a precipitate as well as aqueous Cm(III)–phosphate species coexist in solution. This will require careful planning of the experiments as the amount of aqueous Cm(III) must be determined reliably to allow for the subsequent thermodynamic calculations, which requires a separation method such as ultracentrifugation, capable of removing nanoparticulate matter without introducing foreign substances into the system, i.e. from nanoporous filter materials. Thus, the further exploration of aqueous Cm(III)–phosphate species such as the formation of 1:1 and/or 1:2 $Cm(HPO_4)^+$ and $Cm(HPO_4)_2^-$ complexes must be the scope of well–designed future studies.

## 4 Conclusions

In this study we investigated the complexation of Cm(III) with aqueous phosphates using luminescence spectroscopy as speciation tool. Three complexes could be identified in the phosphate–containing solutions, namely $Cm(H_2PO_4)^{2+}$, $Cm(H_2PO_4)_2^+$, and $Cm(HPO_4)^+$. For the former two complexes, present in sufficient abundancy, conditional complexation constants at several ionic strengths (0.5–3.0 $mol \cdot L^{-1}$ $NaClO_4$) could be derived, which were extrapolated to standard conditions using the specific ion interaction theory (SIT). This way ion interaction coefficients $\varepsilon(Cm(H_2PO_4)_n^{(3-n)+};ClO_4^-)$ (n = 1,2) for the charged Cm(III)–phosphate species interacting with the electrolyte anions could be obtained. Temperature–dependent complexation constants were derived from luminescence data collected in the temperature–range 25–90 °C. By applying the integrated and extended van't Hoff equations, the molal enthalpy $\Delta_R H_m^0$ and molal entropy $\Delta_R S_m^0$ of reaction for the two Cm(III)–phosphate complexes could be derived. For the $Cm(H_2PO_4)^{2+}$ species, the temperature–dependent data was well described with the former equation, while a better fit was obtained for $Cm(H_2PO_4)_2^+$, when including the standard molal heat capacity of reaction. The underlying reason for this different temperature–dependent behavior could be a slightly different coordination chemistry of these complexes. By combining *ab initio* calculations with a thorough analysis of the obtained luminescence spectroscopic data, we could show that both $Cm(H_2PO_4)^{2+}$ and $Cm(H_2PO_4)_2^+$ complexes with an overall CN of 9 are stable in solution at 25 °C. This coordination is preserved for the former complex in the investigated temperature range up to 90 °C. For the latter complex an increasing amount of 8–fold coordinated species could be established with increasing temperature. Such a coordination change may be of relevance for

the complexation of f–elements with several other inorganic and/or organics systems which to date have only been described with one overall complex configuration. With the development of new computational tools and sensitive spectroscopic methods, the possibility for derivation of individual thermodynamic data for complexes in different coordination, to accurately describe the speciation of inorganic and organic complexes and their temperature–dependent behavior in aqueous systems, should be explored.

# 5 Experimental section

## 5.1 Sample preparation

### *5.1.1 Reagents*

All solutions used in the present study were prepared from high purity reagent grade materials without further purification or treatment. $NaClO_4 \cdot H_2O$ (Sigma–Aldrich, p.a., ACS reagent, ≥ 99.5%) and ortho–phosphoric acid (85% from Merck, Suprapur) were used as background electrolyte and phosphate source in the samples, respectively. For the dilution of all solutions to the desired concentrations, doubly deionized water (MilliQ) was used. As curium source a $1\times10^{-5}$ mol·L$^{-1}$ $^{248}$Cm stock solution in 0.01 mol·L$^{-1}$ $HClO_4$ was applied. Note: $^{248}$Cm is a radionuclide with a half–life of $3.48 \times 10^5$ years, decaying through α–emission (92%) and spontaneous fission (8%). The use of $^{248}$Cm requires the appropriate infrastructure and personnel trained in the handling of α–emitting isotopes. All pH–adjustments were conducted with 0.5 – 5.0 mol·L$^{-1}$ $HClO_4$ (Sigma Aldrich, p.a) and 2.0 – 5.0 mol·L$^{-1}$ NaOH (Carl Roth, ≥ 99%) solutions.

### *5.1.2 Cm(III)–phosphate samples*

To account for the Cm(III) speciation at 25 °C in the presence of aqueous phosphates, investigations were conducted at different pH–values and ionic strengths. Due to the very low solubility of reported actinide or lanthanide phosphates such as crystalline $LnPO_4 \cdot 0.667\ H_2O$ rhabdophane (*Ln* = La to Dy) with $\log_{10}$ K°$_{sp}$ (25 °C) ranging from –25.6 ± 0.8 (Pr) to –24.9 ± 1.7 (Eu)[38] and amorphous $AmPO_4 \cdot xH_2O$ with $\log_{10}$ K°$_{sp}$ (25 °C) = –24.79 ± 0.18,[37] the first set of experiments was conducted at rather acidic conditions of $-\log_{10}[H^+] = 2.52$. At this pH–value and ionic strengths of 0.5, 1.0, and 2.0 mol·L$^{-1}$, the solubility product of Cm–rhabdophane will not be exceeded for a total Cm(III) concentration of $8.76\times10^{-8}$–$1.15\times10^{-7}$ mol·L$^{-1}$ and total phosphate concentrations [Σ($PO_4$)] up to 0.055 mol·L$^{-1}$ used in the experiments. At this low pH, however, the phosphate speciation is dominated by the $H_2PO_4^-$

ligand, while the overall $HPO_4^{2-}$ concentration, even in the samples with 0.055 mol·L$^{-1}$ phosphate remains very low, at approximately $3\times10^{-6}$ mol·L$^{-1}$. Therefore, in order to increase the amount of $HPO_4^{2-}$ in solution, a second set of experiments was conducted at a higher pH of $-\log_{10}[H^+] = 3.44$ (I = 1.0 and 2.4 mol·L$^{-1}$) or 3.65 (I = 3.0 mol·L$^{-1}$). In these experiments, the overall curium concentration was decreased to $1.15\times10^{-8}$ mol·L$^{-1}$ to suppress the formation of Cm–rhabdophane, while the total phosphate concentration was kept below 0.08 mol·L$^{-1}$.

All above–mentioned samples, independent of the pH, were prepared by mixing $NaClO_4$ and $H_3PO_4$ to the desired overall ionic strength and phosphate concentrations, respectively. Thereafter the sample pH was adjusted by adding appropriate amounts of either $HClO_4$ or NaOH to the samples. The measured pH ($pH_{exp}$) was corrected for ionic strength effects using Eq. 14 below, to obtain the actual molar $H^+$ concentration.

$$-\log_{10}[H^+] = pH_{exp} + A_c \qquad \text{(Eq. 14)}$$

The coefficient $A_c$ was determined based on Eq. 15 derived in our previous study,[16] where I is the ionic strength in mol·L$^{-1}$.

$$A_c = 0.0127 \cdot I^2 + 0.1568 \cdot I + 0.0606 \qquad \text{(Eq. 15)}$$

The pH–measurements were done with combination pH electrodes (SenTix MIC from VWR). In order to avoid precipitation of $KClO_4$ in the diaphragm of the electrode, the original junction electrolyte (3 mol·L$^{-1}$ KCl) was replaced by 3 mol·L$^{-1}$ NaCl solution (Carl Roth, ≥ 99.5 %). The electrodes were calibrated using standard buffer solutions (WTW). After an equilibration time of at least one day, the sample pH was remeasured and readjusted if necessary, followed by addition of 5 – 50 µL of Cm(III) stock solution to the samples. After Cm(III) addition, no additional pH–adjustment was undertaken to avoid rhabdophane precipitation as a result of NaOH addition to the samples.

To investigate the impact of elevated temperature on the Cm(III)–phosphate complexation reaction, the solutions prepared at I = 1.0 mol·L$^{-1}$ and $-\log_{10}[H^+] = 2.52$ were taken and stepwise heated up to 90 °C using a HLCThermoMixer (MKR 23 BlockThermostate, Ditabis). All experimental conditions have been summarized in Table 9.

Table 9: Overview of the experimental conditions used in the various Cm(III)–phosphate complexation rows.

| $-\log_{10}[H^+]$ | I ($mol \cdot L^{-1}$) | T (°C) | [Cm(III)] ($mol \cdot L^{-1}$) | $[\Sigma(PO_4)]_{max}$ ($mol \cdot L^{-1}$) |
|---|---|---|---|---|
| 2.52 | 0.5 | 25 | $1.15 \times 10^{-7}$ | 0.055 |
| 2.52 | 2.0 | 25 | $8.76 \times 10^{-8}$ | 0.04 |
| 2.52 | 1.0 | 25–90 | $1.15 \times 10^{-7}$ | 0.055 |
| 3.44 | 1.0 | 25 | $1.15 \times 10^{-8}$ | 0.070 |
| 3.44 | 2.4 | 25 | $1.15 \times 10^{-8}$ | 0.08 |
| 3.65 | 3.0 | 25 | $1.15 \times 10^{-8}$ | 0.040 |

### 5.2 Speciation calculations

The determination of the complexation constants via slope analysis requires the molality of free $H_3PO_4$, which was calculated using the geochemical speciation software Phreeqc.[39] The activity coefficients were treated by the SIT approach using the ThermoChimie dataset (version 9b0) from Andra.[40] All calculations were performed with chemical conditions (ionic strength, total phosphate concentration, $-\log_{10}[H^+]$, and temperature) identical to those applied in the experiments.

### 5.3 Luminescence spectroscopy

Luminescence spectroscopy was used to study the complexation reaction between Cm(III) and phosphates. After addition of Cm(III) to the phosphate containing samples, measurements were undertaken within a day to avoid sample aging and the possibility of rhabdophane precipitation over time. For the luminescence spectroscopic measurements, 3 mL of the sample were transferred into a quartz glass cuvette with PTFE stopper. To ensure complete tightness of the cuvettes during the high–temperature measurements, a semitransparent, thermoplastic film was wrapped around the cuvette stoppers and exchanged if necessary. The desired temperature was achieved by pre–equilibrating the samples in block thermostats (HLCThermoMixer, MKR 23 Ditabis), followed by an additional equilibration time of at least 10 minutes in a heatable cuvette house. The luminescence spectroscopic investigations were conducted with a dye laser set–up (NarrowScan, Radiant Dyes), coupled to a Nd:YAG (Continuum, Surelite) pump laser. The dye consisted of a 1:1 mixture of Exalite 389 and Exalite 398. Cm(III) luminescence emission spectra were recorded between 570 and 615 nm (1200 $lines \cdot mm^{-1}$, Cm(III)–phosphate rows at $-\log_{10}[H^+] = 2.52$) or 560 and 630 nm (600

lines·mm$^{-1}$, Cm(III)–phosphate rows at $-\log_{10}[H^+]$ = 3.44–3.65), 1 µs after the exciting laser pulse with a constant excitation wavelength of 396.6 nm. The laser pulse energy was measured by a pyroelectric energy sensor and was found to be between 3 and 5 mJ in each measurement. Luminescence emission was detected by an optical multichannel analyzer (Shamrock 303i) and an ICCDCamera (iStar, Andor). Luminescence lifetime measurements were collected for selected samples, by recording the luminescence emission as a function of delay time between the laser pulse and the camera gating. A delay increment between 5 and 7 µs were used for overall delay times of 260 µs.

The collected luminescence data was treated with the programs Matlab[41] (2019, version 2) and OriginPro[42] (version 2019). Matlab was used to integrate the collected luminescence emission spectra as a function of delay time to obtain luminescence lifetime decay curves. Origin was used for the stepwise extraction of pure component spectra from the measured composite spectra. The calculation of the Cm(III)–phosphate species distribution was done with MS Excel using a least squares fitting method described in detail in Huittinen et al. (2012)[43] and Eibl et al. (2019).[44] Luminescence intensity (LI) factors for the correction of relative luminescence intensity variations of the present species was done by comparing the intensity of the uncomplexed Cm(III) aquo ion with the measured Cm(III)–phosphate spectra, and by fitting the LI factors using the same least squares fit approach. Eventually, the obtained pure component spectra (aquo ion and Cm(III)–phosphate complexes) were fitted with four Lorentzian peaks describing the emission from the four crystal field states (denoted $A_1$–$A_4$ by convention) of the emitting electronic level back to the ground state. For the fit, the area under the peak (population of the crystal field levels) was constrained to follow the Boltzmann distribution given by Eq. 16.

$$\frac{N_f}{N_i} = \exp\left(-\frac{\Delta E}{k_B T}\right) \qquad \text{(Eq. 16)}$$

$N_f$ and $N_i$ refer to the population of the various crystal field levels of the excited state and the ground state, respectively. $\Delta E$ is the band gap between the excited state and the ground state ($\Delta E = hc\left(\frac{1}{\lambda_f} - \frac{1}{\lambda_i}\right)$, h = Planck constant ($6.62607\times10^{-34}$ J·s), c = the speed of light in vacuum (2.99792 m·s$^{-1}$), and $\lambda$ = emission wavelength in meters), T is the temperature in Kelvin and $k_B$ the Boltzmann constant ($1.38065\times10^{-23}$ J·K$^{-1}$). To reduce the number of free variables in the fit, the FWHM of two consecutive transitions was constrained to follow FWHM ($A_{n+1}$) ≥ FWHM ($A_n$), n = 1–3.

The fitted peak positions were thereafter used to compare the experimental crystal field splitting with the computed ones, as it was earlier in the text, section 2.3.

### 5.4 *Ab initio* simulations

In the present study, *ab initio* simulations were conducted to i) investigate the chemical bond properties as a function of the number of ligands, and ii) to shed light on the spectroscopic properties by the means of excited–state electronic structure calculations. In this aim, the geometries of the various species involved in the complexation processes, *i.e.*, $H_2PO_4^-$, $H_3PO_4$, $[Cm(H_2O)_{8,9}]^{3+}$, $[Cm(H_2O)_{7,8}(H_2PO_4)]^{2+}$ and $[Cm(H_2O)_{6,7}(H_2PO_4)_2]^{+}$ were optimized. The appropriate thermodynamic corrections including enthalpy, entropy, solvent effects, as well as the spin–orbit coupling contributions to estimate the Gibbs free energy values of the complexation reactions were applied. For each Cm–containing species, the absorption and emission transitions were computed.

#### *5.4.1 Structures, bonding analysis, thermodynamic corrections and solvent correction*

The structures used for the $H_2O$, $H_2PO_4^-$, $H_3PO_4$, $[Cm(H_2O)_{8,9}]^{3+}$, $[Cm(H_2O)_{7,8}(H_2PO_4)]^{2+}$, and $[Cm(H_2O)_{6,7}(H_2PO_4)_2]^{+}$ species were optimized using the second order Møller–Plesset perturbation theory (MP2) and Unrestricted MP2 methods for the open–shell systems combined with Resolution of the Identity[45, 46] with the appropriate atomic auxiliary basis functions.[47, 48] For the Cm(III) complexes, a high–spin octet state was considered by occupying the seven 5*f* orbitals of Cm(III) cation by the 7 unpaired electrons. Relativistic small–core pseudo potential (60 e– in core) of the Stuttgart–Cologne group were employed associated with the def2–TZVP basis sets (14s13p10d8f) / [10s9p5d4f3g] for the Cm(III) cation.[49] Identical basis sets quality was considered for the lighter elements in all molecules.[50]

To analyze the nature of the curium–ligand chemical bonds the quantum theory of atoms–in–molecules (QTAIM) analysis was applied. In this context the Gaussian 16 (Revision B01) quantum chemistry package[51] with the same basis sets was used to generate the appropriate wave–function extended files (wfx) to be used by the AIMAll package.[52] To estimate harmonic vibrational partition functions at 25 °C and 90 °C and 0.1 MPa, which are necessary to calculate the enthalpic and entropic contributions to the gas–phase energies, numerical frequency calculations were also performed.

The Conductor–like screening model–Real Solvents (COSMO) model[53] was applied to compute the solvation Gibbs free energies at the two different temperatures using two

dielectric constants for the water solvent $\varepsilon_r$ = 78 at 25 °C and $\varepsilon_r$ = 58 at 90 °C, respectively. All the calculations were performed with the Turbomole 7.4.1 package.[54, 55]

### *5.4.2 Predictions of the ground–state energies and spectroscopic calculations*

To derive the most accurate ground–state energies of Cm(III) complexes, and to compute the transition energies of the excited states, state–averaged CASSCF (complete–active–space self–consistent field) scalar relativistic calculations with the Douglas–Kroll–Hess Hamiltonian[56, 57] were performed for all the possible multiplicities encountered for seven unpaired 5f electrons, i.e., 1 octet, 48 sextets, 392 quartets, 784 doublets states. Spin–orbit coupling contributions to the gas–phase energies were computed with the Restricted Active Space State Interaction (RASSI) approach,[58] by coupling all CASSCF wave functions, while dynamical correlation contributions to the ground–state energies were accounted for with the XMS–CASPT2 approach (multi–state complete active space second–order perturbation theory) only for Cm(III) complexes, as light molecules are treated with the single–reference MP2 method. In the MP2 and XMS–CASPT2 calculations, the 1s core orbitals of the oxygen atoms, and up to the 5s, 5p, 5d orbitals of the actinide ions were kept frozen. Absorption and emission energies were computed shifting the energy of the excited states obtained at the SO–CASSCF level, by a quantity that corresponds to the energy difference of the first sextet state obtained at the CASSCF and XMS–CASPT2 levels. Note that it was impossible to perform XMS–CASPT2 calculations for the other multiplicities (quartets and doublets) as the states were too numerous. All HF/CASSCF and MP2/XMS–CASPT2 ground–state energies were extrapolated to the Complete Basis Set limit (CBS limit), from calculations using the all–electron Atomic Natural Orbital relativistic core correlation (ANO–RCC) basis sets optimized by Roos et al.[59, 60] with triple–zeta and quadruple–zeta basis sets, and applying two–point extrapolation formulas.[61-63] These relativistic wave–function calculations were performed with the OpenMolcas program.[64, 65]

### *5.4.3 Composite method for thermodynamic estimations and chemical reactions*

To estimate the $\Delta G_r^\circ(T)$ for the following reactions (n = 9),

$$[Cm(H_2O)_n]^{3+} \rightarrow [Cm(H_2O)_{n-1}]^{3+} + H_2O \qquad \text{(R–3)}$$

$$[Cm(H_2O)_{n-1}(H_2PO_4)]^{2+} \rightarrow [Cm(H_2O)_{n-2}(H_2PO_4)]^{2+} + H_2O \qquad \text{(R–4)}$$

$$[Cm(H_2O)_{n-2}(H_2PO_4)_2]^{+} \rightarrow [Cm(H_2O)_{n-3}(H_2PO_4)_2]^{+} + H_2O \qquad \text{(R–5)}$$

one has to determine the Gibbs free energy associated to each reactant and product by adding all contributions listed below.

$$G(A,T) = E^{CBS}_{XMS-CASPT2}(A) + E^{SO}(A) + G^{gaz}_{coor}(A,T) + G^{sol}(A,T)$$

For a compound A, these contributions encompass the CBS extrapolated scalar relativistic electronic energy ($E^{CBS}_{XMS-CASPT2}(A)$), the spin–orbit contribution $E^{SO}(A)$ for the Cm(III) complexes, Gibbs free energy correction $G^{gaz}_{coor}(A,T)$, and the hydration Gibbs free energy $G^{sol}(A,T)$. Note that for all these reactions listed above, a correction of RT ln(55.34) needs to be added to account for the change of standard state for the released water molecule from pure water (concentration of 55.34 mol·L$^{-1}$) to reference standard state 1 mol·L$^{-1}$.[66]

## 6 Conflicts of interest

There are no conflicts to declare.

## 7 Acknowledgements

This work was supported by the German Federal Ministry of Education and Research (BMBF), Project No. 02NUK039B (ThermAc) and 033R127D (SEM$^2$). F. Réal and V. Vallet acknowledge support by the French government through the Program "Investissement d'avenir" (LABEX CaPPA / ANR–11–LABX–0005–01 and I–SITE ULNE / ANR–16–IDEX–0004 ULNE), as well as by the Ministry of Higher Education and Research, Hauts de France Council and European Regional Development Fund (ERDF) through the Contrat de Projets État–Région (CPER –CLIMIBIO). Furthermore, this work was granted access to the HPC resources of [CINES/IDRIS/TGCC] under the allocation 2019–2020 [A0070801859] made by GENCI.

## 8 References


1. E. Nahas, *World Journal of Microbiology & Biotechnology*, 1996, **12**, 567-572.
2. D. L. Jones and E. Oburger, in *Phosphorus in Action: Biological Processes in Soil Phosphorus Cycling*, eds. E. Bünemann, A. Oberson and E. Frossard, Springer Berlin Heidelberg, Berlin, Heidelberg, 2011, pp. 169-198.
3. H. Holtan, L. Kampnielsen and A. O. Stuanes, *Hydrobiologia*, 1988, **170**, 19-34.
4. A. N. Sharpley, T. C. Daniel and D. R. Edwards, *Journal of Production Agriculture*, 1993, **6**, 492-500.
5. J. T. Sims, R. R. Simard and B. C. Joern, *Journal of Environmental Quality*, 1998, **27**, 277-293.
6. Z. Yuan, J. Shi, H. Wu, L. Zhang and J. Bi, *Journal of Environmental Management*, 2011, **92**, 2021-2028.
7. R. C. Ewing and L. Wang, *Reviews in Mineralogy and Geochemistry*, 2002, **48**, 673-699.
8. E. H. Oelkers and J.-M. Montel, *Elements*, 2008, **4**, 113-116.
9. N. Dacheux, N. Clavier and R. Podor, *American Mineralogist*, 2013, **98**, 833-847.
10. N. Huittinen, A. C. Scheinost, Y. Ji, P. M. Kowalski, Y. Arinicheva, A. Wilden, S. Neumeier and T. Stumpf, *Inorganic Chemistry*, 2018, **57**, 6252-6265.
11. A. Kumari, R. Panda, M. K. Jha, J. R. Kumar and J. Y. Lee, *Minerals Engineering*, 2015, **79**, 102-115.
12. S. X. Wu, L. S. Wang, L. S. Zhao, P. Zhang, H. El-Shall, B. Moudgil, X. W. Huang and L. F. Zhang, *Chemical Engineering Journal*, 2018, **335**, 774-800.
13. W. Runde, *Los Alamos Science*, 2000, **26**, 392-411.
14. R. J. Silva and H. Nitsche, *Radiochimica Acta*, 1995, **70/71**, 377-396.
15. K. Maher, J. R. Bargar and G. E. Brown, *Inorganic Chemistry*, 2013, **52**, 3510-3532.
16. N. Jordan, M. Demnitz, H. Losch, S. Starke, V. Brendler and N. Huittinen, *Inorganic Chemistry*, 2018, **57**, 7015-7024.
17. H. Moll, V. Brendler and G. Bernhard, *Radiochimica Acta*, 2011, **99**, 775-782.
18. A. Morgenstern, Ph.D. thesis, Technische Universität München, Garching, 1997.
19. A. I. Moskvin, *Soviet Radiochemistry*, 1969, **11**, 447-449.
20. V. K. Rao, G. R. Mahajan and P. R. Natarajan, *Radiochimica Acta*, 1986, **40**, 145-149.
21. M. S. Borisov, A. A. Elesin, I. A. Lebedev, V. T. Filimonov and G. N. Yakovlev, *Soviet Radiochemistry*, 1966, **8**, 40-44.

22. I. A. Lebedev, V. Y. Frenkel, Y. M. Kulyako and B. F. Myasoedov, *Soviet Radiochemistry*, 1979, **21**, 692-698.
23. R. J. Lemire, D. A. Palmer, P. Taylor and H. Schlenz, *Chemical Thermodynamics of Iron: Part 2.*, OECD Publications, Paris, 2020.
24. R. J. Silva, G. Bidoglio, M. H. Rand, P. B. Robouch and H. P. Wanner, I., *Chemical Thermodynamics of Americium*, Elsevier, North-Holland, 1995.
25. A. I. Moskvin, *Soviet Radiochemistry*, 1971, **13**, 688-693.
26. T. Kimura and G. R. Choppin, *Journal of Alloys and Compounds*, 1994, **213-214**, 313-317.
27. O. Söhnel and P. Novotný, *Densities of aqueous solutions of inorganic substances*, Elsevier, Amsterdam, 1985.
28. R. C. M. van Aert and D. Jackson, *Research Synthesis Methods*, 2019, **10**, 515-527.
29. H. C. Moog and W. Voigt, *Thermodynamic Reference Database. Dielectric Constant, Vapor Pressure, and Density of Water and the Calculation of Debye-Hückel Parameters $A_{DH}$, $B_{DH}$, and $A^{\phi}$ for Water. THEREDA Technical Paper*, 2011.
30. Q. R. Huang, J. R. Kingham and N. Kaltsoyannis, *Dalton Transactions*, 2015, **44**, 2554-2566.
31. A. Kerridge, *Chemical Communications*, 2017, **53**, 6685-6695.
32. P. Lindqvist-Reis, F. Real, R. Janicki and V. Vallet, *Inorganic Chemistry*, 2018, **57**, 10111-10121.
33. P. Lindqvist-Reis, R. Klenze, G. Schubert and T. Fanghänel, *The Journal of Physical Chemistry B*, 2005, **109**, 3077-3083.
34. N. L. Banik, V. Vallet, F. Real, R. M. Belmecheri, B. Schimmelpfennig, J. Rothe, R. Marsac, P. Lindqvist-Reis, C. Walther, M. A. Denecke and C. M. Marquardt, *Dalton Transactions*, 2016, **45**, 453-457.
35. Y. S. Qiao, D. C. Sergentu, H. L. Yin, A. V. Zabula, T. Cheisson, A. McSkimming, B. Manor, P. Carroll, J. Anna, J. Autschbach and E. Schelter, *Abstracts of Papers of the American Chemical Society*, 2018, **256**, 2.
36. P. L. Geissler, *Journal of the American Chemical Society*, 2005, **127**, 14930-14935.
37. D. Rai, A. R. Felmy and R. W. Fulton, *Radiochimica Acta*, 1992, **56**, 7-14.
38. C. Gausse, S. Szenknect, D. W. Qin, A. Mesbah, N. Clavier, S. Neumeier, D. Bosbach and N. Dacheux, *European Journal of Inorganic Chemistry*, 2016, **2016**, 4615-4630.
39. D. L. Parkhurst and C. A. J. Appelo, *Description of input and examples for PHREEQC version 3—A computer program for speciation, batch-reaction, one-*

*dimensional transport, and inverse geochemical calculations*, U.S. Geological Survey Techniques and Methods, book 6, chap. A43, 2013.

40. E. Giffaut, M. Grivé, P. Blanc, P. Vieillard, E. Colàs, H. Gailhanou, S. Gaboreau, N. Marty, B. Madé and L. Duro, *Applied Geochemistry* 2014, **49**, 225–236.
41. *MATLAB 2019 (Version 2)*, Natick, Massachusetts, United States, 2019.
42. *OriginPro, Version 2019*, Northampton, MA, USA, 2019.
43. N. Huittinen, T. Rabung, A. Schnurr, M. Hakanen, J. Lehto and H. Geckeis, *Geochimica et Cosmochimica Acta*, 2012, **99**, 100-109.
44. M. Eibl, S. Virtanen, F. Pischel, F. Bok, S. Lönnrot, S. Shaw and N. Huittinen, *Applied Surface Science*, 2019, **487**, 1316-1328.
45. C. Hättig, A. Hellweg and A. Köhn, *Physical Chemistry Chemical Physics*, 2006, **8**, 1159–1169.
46. C. Hättig and F. Weigend, *The Journal of Chemical Physics*, 2000, **113**, 5154-5161.
47. F. Weigend, A. Köhn and C. Hättig, *The Journal of Chemical Physics*, 2002, **116**, 3175-3183.
48. C. Hättig, *Physical Chemistry Chemical Physics*, 2005, **7**, 59-66.
49. X. Cao and M. Dolg, *Journal of Molecular Structure: THEOCHEM*, 2004, **673**, 203-209.
50. F. Weigend, M. Häser, H. Patzelt and R. Ahlrichs, *Chemical Physics Letters*, 1998, **294**, 143-152.
51. M. J. Frisch, G. W. Trucks, H. B. Schlegel, G. E. Scuseria, M. A. Robb, J. R. Cheeseman, G. Scalmani, V. Barone, G. A. Petersson, H. Nakatsuji, X. Li, M. Caricto, A. V. Marenich, J. Bloino, B. G. Janesko, R. Gomperts, B. Mennucci, H. P. Hratchian, J. V. Ortiz, A. F. Izmaylov, J. L. Sonnenberg, D. Williams-Young, F. Ding, F. Lipparini, F. Egidi, J. Goings, B. Peng, A. Petrone, T. Henderson, D. Ranasinghe, V. G. Zakrzewski, J. Gao, N. Rega, G. Zheng, W. Liang, M. Hada, M. Ehara, K. Toyota, R. Fukuda, J. Hasegawa, M. Ishida, T. Nakajima, Y. Honda, O. Kitao, H. Nakai, T. Vreven, K. Throssell, J. A. Montgomery, Jr., J. E. Peralta, F. Ogliaro, M. J. Bearpark, J. J. Heyd, E. N. Brothers, K. N. Kudin, V. N. Staroverov, T. A. Keith, R. Kobayashi, J. Normand, K. Raghavachari, A. P. Rendell, J. C. Burant, S. S. Iyengar, J. Tomasi, M. Cossi, J. M. Millam, M. Klene, C. Adamo, R. Cammi, J. W. Ochterski, R. L. Martin, K. Morokuma, O. Farkas, J. B. Foresman and D. J. Fox, *Gaussian 16, Revision B.01*, Wallingford CT, 2016.

52. A. Todd and T. K. Keith, *AIMAll (Version 17.11.14)*, Gristmill Software (aim.tkgristmill.com), Overland Park KS, USA, 2019.
53. A. Klamt and G. Schüürmann, *Journal of the Chemical Society-Perkin Transactions 2*, 1993, 799-805.
54. S. G. Balasubramani, G. P. Chen, S. Coriani, M. Diedenhofen, M. S. Frank, Y. J. Franzke, F. Furche, R. Grotjahn, M. E. Harding, C. Hattig, A. Hellweg, B. Helmich-Paris, C. Holzer, U. Huniar, M. Kaupp, A. M. Khah, S. K. Khani, T. Muller, F. Mack, B. D. Nguyen, S. M. Parker, E. Perlt, D. Rappoport, K. Reiter, S. Roy, M. Ruckert, G. Schmitz, M. Sierka, E. Tapavicza, D. P. Tew, C. van Wullen, V. K. Voora, F. Weigend, A. Wodynski and J. M. Yu, *Journal of Chemical Physics*, 2020, **152**, 36.
55. *TURBOMOLE V7.4.1, a development of University of Karlsruhe and Forschungszentrum Karlsruhe GmbH, 1989-2007, TURBOMOLE GmbH, since 2007; available from* http://www.turbomole.com, 2019.
56. M. Douglas and N. M. Kroll, *Annals of Physics*, 1974, **82**, 89-155.
57. B. A. Hess, *Physical Review A*, 1986, **33**, 3742-3748.
58. P.-A. Malmqvist, B. O. Roos and B. Schimmelpfennig, *Chemical Physics Letters*, 2002, **357**, 230-240.
59. B. O. Roos, R. Lindh, P. A. Malmqvist, V. Veryazov and P. O. Widmark, *Chemical Physics Letters*, 2005, **409**, 295-299.
60. B. O. Roos, R. Lindh, P.-A. Malmqvist, V. Veryazov and P.-O. Widmark, *The Journal of Physical Chemistry A*, 2004, **108**, 2851-2858.
61. D. Feller, *The Journal of Chemical Physics*, 1992, **96**, 6104-6114.
62. D. Feller, *The Journal of Chemical Physics*, 1993, **98**, 7059-7071.
63. A. Karton and J. M. L. Martin, *Theoretical Chemistry Accounts*, 2006, **115**, 330-333.
64. F. Aquilante, J. Autschbach, A. Baiardi, S. Battaglia, V. A. Borin, L. F. Chibotaru, I. Conti, L. De Vico, M. Delcey, I. F. Galvan, N. Ferre, L. Freitag, M. Garavelli, X. J. Gong, S. Knecht, E. D. Larsson, R. Lindh, M. Lundberg, P. A. Malmqvist, A. Nenov, J. Norell, M. Odelius, M. Olivucci, T. B. Pedersen, L. Pedraza-Gonzalez, Q. M. Phung, K. Pierloot, M. Reiher, I. Schapiro, J. Segarra-Marti, F. Segatta, L. Seijo, S. Sen, D. C. Sergentu, C. J. Stein, L. Ungur, M. Vacher, A. Valentini and V. Veryazov, *Journal of Chemical Physics*, 2020, **152**, 25.
65. I. F. Galván, M. Vacher, A. Alavi, C. Angeli, F. Aquilante, J. Autschbach, J. J. Bao, S. I. Bokarev, N. A. Bogdanov, R. K. Carlson, L. F. Chibotaru, J. Creutzberg, N. Dattani, M. G. Delcey, S. J. S. Dong, A. Dreuw, L. Freitag, L. M. Frutos, L. Gagliardi, F.

Gendron, A. Giussani, L. González, G. Grell, M. Y. Guo, C. E. Hoyer, M. Johansson, S. Keller, S. Knecht, G. Kovacevic, E. Källman, G. Li Manni, M. Lundberg, Y. J. Ma, S. Mai, J. P. Malhado, P. A. Malmqvist, P. Marquetand, S. A. Mewes, J. Norell, M. Olivucci, M. Oppel, Q. M. Phung, K. Pierloot, F. Plasser, M. Reiher, A. M. Sand, I. Schapiro, P. Sharma, C. J. Stein, L. K. Sorensen, D. G. Truhlar, M. Ugandi, L. Ungur, A. Valentini, S. Vancoillie, V. Veryazov, O. Weser, T. A. Wesolowski, P. O. Widmark, S. Wouters, A. Zech, J. P. Zobel and R. Lindh, *Journal of Chemical Theory and Computation*, 2019, **15**, 5925-5964.

66. V. S. Bryantsev, M. S. Diallo and W. A. Goddard, *Journal of Physical Chemistry B*, 2008, **112**, 9709-9719.